University of Pardubice

Faculty of Chemical Technology

Department of Physical Chemistry

Production of light olefins via (oxidative) dehydrogenation of light alkanes over nontraditional heterogeneous catalysts

DOCTORAL THESIS

Author: M.Sc. Mehran Sajad

Supervisor: Prof. Ing. Roman Bulanek, Ph.D.

2023

I declare:

The thesis entitled “Production of light olefins via (oxidative) dehydrogenation of light alkanes over nontraditional heterogeneous catalysts” is my own work. All literary sources and information that I used in the thesis are referenced in the bibliography. I have been acquainted with the fact that my work is subject to the rights and obligations arising from Act No. 121/2000 Sb., On Copyright, on Rights Related to Copyright and on Amendments to Certain Acts (Copyright Act), as amended, especially with the fact that the University of Pardubice has the right to conclude a license agreement for the use of this thesis as a school work under Section 60, Subsection 1 of the Copyright Act, and that if this thesis is used by me or a license to use it is granted to another entity, the University of Pardubice is entitled to request a reasonable fee from me to cover the costs incurred for the creation of the work, depending on the circumstances up to their actual amount.

I acknowledge that in accordance with Section 47b of Act No. 111/1998 Sb., On Higher Education Institutions and on Amendments to Other Acts (Act on Higher Education Institutions), as amended, and the Directive of the University of Pardubice No. 7/2019 Rules for Submission, Publication and Layout of Theses, as amended, the thesis will be published through the Digital Library of the University of Pardubice.

In Pardubice, Czech Republic on .....

Mehran Sajad by own hand

ACKNOWLEDGMENTS

I would like to thank the following people:

My supervisor, prof. Ing. Roman Bulánek, Ph.D., for the scientific and moral support during all the years of my Ph.D. study. I want to thank you for your positive and friendly attitude, for the knowledge and advices you have given. Thank you for the motivation to do high quality research.

The rector of the University of Pardubice, prof. Ing. Libor Čapek, Ph.D., for all your help, and supportive and friendly attitude during all years of my Ph.D. study.

My former colleague and great friend, Ing. Diego Valdés, Ph.D., for being a "dream team" during our work, all of your support, and the great time you have given.

My former colleague and great friend, Ing. Jiři Kotera, for all your help, support, and great time.

My great friend Ing. Zuzana Tuťálková, for all your help, positive energy, and great time you have given.

My great friend, M.Sc. Farshid Farzaneh, for all your help, support, and the great time you have given.

My great friend, M.Sc. Nadi Shojaee, for all your help, support, and great time you have given.

My great friend, M.Sc. Nooshin Jafari, for all your help, support, and great time you have given.

My friend, Raul Zazpe, Ph.D, for all your help, advices, positive energy, and great time you have given.

My colleague and friend Ing. Lada Dubnová, for all your help, support, positive energy, and great days.

My colleague and friend Ing. Vendula Meinhardová, for all your support, positive energy, and great days.

My colleague and friend Ing. Helena Drobná, Ph.D. for all your support, positive energy, and great days.

My former colleague and friend, Dr. Yosra Gherib, for all your help, support, and great days.

My friend, Caroline Novák-Jolly, for all your help, support, and great days.

My colleague and friend, Dr. Safaa Essid, for all your help, support, and great days.

My friend, Hanna Sopha, Ph.D., for all your help, support, and great time you have given.

My former colleague Ing. Jan Vaculík, Ph.D., for all your help.

My colleague Ing. Kateřina Knotková, Ph.D., for all your help.

All members and students of our department for their help and useful discussions.

The financial support by the Czech Science Foundation (project No. 22-23120S) is greatly acknowledged. The Center of Materials and Nanotechnologies of the University of Pardubice is greatly acknowledged for all their supports.

Last but not least, My family for their love and support during my PhD journey.

سپاسگزاری

تقدیر و تشکر بی کران خود را تقدیم میکنم به عزیزانی که در تمام مدت دوره دکتری حمایت بی دریغ ایشان برای من گرما بخش این مسیر طولانی و پر پیچ و خم بوده و از وجود پر مهر ایشان به خود میبالم.

به پاس عاطفه سرشار و گرمای امیدبخش وجودشان، و به پاس قلب های بزرگشان.

این پایان نامه و ماحصل آموخته هایم را تقدیم می کنم:

به مادرمهربان و فداکار و عزیز تر از جانم، که هرچه آموختم در مکتب عشق شما آموختم و هرچه بکوشم قطره ای از دریای بی کران مهربانیتان را سپاس نتوانم بگویم. امروز هستی ام به امید شماست و فردا کلید باغ بهشتم رضای شما. ره آوردی گران سنگ تر از این ارزان نداشتم تا به خاک پایتان نثار کنم، باشد که حاصل تلاشم، نسیم گونه، غبار خستگیتان را بزداید. بوسه بر دستان پرمهرتان.

به پدرم که مهر آسمانی شان آرام بخش آلام زمینی ام است و استوارترین تکیه گاهم، دستان پرمهرش بود.

به خواهر عزیزم فخری سجاد که همواره با قلبی بزرگ و مهری بی انتها یار و یاور من بوده و ذره ای از زحمات گرانقدرش جبران پذیر نخواهد بود.

به برادر عزیزم مهرداد سجاد که همیشه بیش از یک برادر، دوست و رفیق، یار و یاور من بوده است.

به برادر عزیزم محمد سجاد که قلب مهربانش به بزرگی آسمان بی کران است.

به همسر و یار خواهرم رضا صادقی که حضور پر مهرش بی انتها و دلسوزی های برادرانه اش همیشه دل گرم کننده بوده است.

به خواهر زاده عزیزم آرزو صادقی که همچون قلبی دیگر در زندگی من میتپد و دنیاهای گره خورده ما جدا نشدنی است.

به خواهر زاده عزیزم علی صادقی که گویی رفیقی عزیز تر از جان شیرین و برادری همراه تا به انتهای همه مسیر هاست.

از همه شما عزیزان سپاسگزارم و تا ابد قدردان حضور و محبت بی دریغ شما هستم.

مهران سجاد

.

ABSTRACT

Light olefins are essential feedstock for industrial processes such as the production of polymers, oxygenates, etc. Currently, these olefins are produced mainly via steam cracking and fluid catalytic cracking of petroleum derivatives. However, the present methods are carried out under severe reaction conditions at high temperatures with significant amounts of CO_2 emission. Moreover, the side products of these processes are alkanes that typically burn, while they have great potential for being used in a more helpful way. On the other hand, the abundant discovery of natural and shale gas around the world has provided another source to meet the highly growing global demand for light olefins. Therefore, the (oxidative) dehydrogenation of light alkanes is growing important way to produce olefins more efficiently. Although direct dehydrogenation of light alkanes has found its way into the industry (but suffering from strong deactivation), oxidative dehydrogenation has not yet been industrially implemented because of the low selectivity problem of the available catalysts due to the overoxidation of the products.

Recently, the supported alkali chlorides and hexagonal boron nitride have shown high activity and selectivity in the oxidative dehydrogenation of light alkanes. Meanwhile, supported noble-metal nanoparticles are considered to be active for the direct dehydrogenation of light alkanes. However, a detailed investigation of the structure-activity-stability relationship for their use in the reaction is required. This thesis focuses on studying the catalytic behavior of these three promising catalyst groups for the (oxidative) dehydrogenation of light alkanes and understanding the phenomena that could influence their activity. In this work, critical parameters such as chemical composition, crystallinity, textural properties, reaction conditions, pretreatment/regeneration effect, stability, catalytic activity, and selectivity of the catalysts in olefin production via alkane (oxidative) dehydrogenation were investigated. A comprehensive characterization with fresh and spent catalysts was considered to explore the physicochemical changes that occurred during the reaction.

In the study of supported alkali chlorides, it was found that the high yield of olefin production by the reported catalytic systems, which is due to a molten layer of mixed salts formed at the reaction temperature, is constrained by deactivation. A comprehensive characterization provided insight into the deactivation mechanism and revealed that chlorine loss in some forms of chlorinated hydrocarbons causes the deactivation.

With respect to the supported noble metal nanoparticles, there are several different methods for encapsulating the metal nanoparticles. One of the recent approaches is the assembly disassembly organization reassembly technique, known as ADOR. In this research, the ADOR method was used to encapsulate Pd nanoparticles within IPC-2 and IPC-4 zeolites. It revealed that layered zeolites with thin

layers, such as UTL, are not suitable supports for the confinement of metallic nanoparticles because the zeolite framework cannot tolerate the severe conditions of the cyclic dehydrogenation reaction and regeneration. Nevertheless, metal nanoparticle confinement is an effective way to prevent sintering and improve the catalytic activity of the supported metal nanoparticles compared to conventional impregnation. Therefore, the confinement may result in better stability performance within zeolitic structures having thicker layers.

Lastly, a new promising nonmetallic catalyst, hexagonal boron nitride, was studied systematically in the oxidative dehydrogenation of propane to have a better understanding of the actual driver and the phenomena involved in this complicated system. This catalyst exhibited high activity and selectivity that was accompanied by the production of ethene as a valuable side product, along with low overoxidation of the products. Although the catalysts undergo substantial changes in chemical composition, textural properties, and crystallinity during the reaction, the activity and selectivity remain almost constant. Unlike previous studies that reported the oxygen content as the main factor, in this work it is shown that the reaction is driven mostly by gas-phase chemistry. Therefore, a longer residence time in a larger free space is essential for radical generation and propagation to improve productivity, while oxygen content does not play a key role. In fact, the change in oxygen content is the result of radical formation and not the cause. This catalyst is privileged because a coupled surface-mediated gas-phase mechanism is involved, resulting in higher activity and productivity compared with traditional metallic catalysts in the oxidative dehydrogenation of light alkanes suffering from overoxidation and low selectivity. It seems that one of the actual roles of hBN is to terminate the generated radicals or adsorption of water, which are formed in the gas phase, to form the products or maybe generate the in situ oxygenated species that eventually result in the formation of products. It is hypothesized that in this system, the initiation stage is in the gas phase and not on the surface of the catalyst.

KEYWORDS

Oxidative dehydrogenation, direct dehydrogenation, heterogeneous catalyst, light alkane, light olefin, characterization.

ABSTRAKT

Lehké olefiny jsou nezbytnou surovinou pro průmyslové procesy, jako je výroba polymerů, oxygenátů atd. V současné době se tyto olefiny vyrábějí především parním krakováním a fluidním katalytickým krakováním ropných derivátů. Předkládané způsoby se však provádějí za náročných reakčních podmínek při vysokých teplotách s významným množstvím emisí CO_2. Kromě toho jsou vedlejšími produkty těchto procesů alkany, které se obvykle spalují, přičemž mají velký potenciál pro užitečnější využití. Na druhou stranu, hojné objevy přírodního a břidlicového plynu po celém světě poskytly další zdroj pro uspokojení vysoce rostoucí celosvětové poptávky po lehkých olefinech. Proto se (oxidativní) dehydrogenace lehkých alkanů stává stále důležitějším způsobem, jak efektivněji vyrábět olefiny. Ačkoli si přímá dehydrogenace lehkých alkanů našla cestu do průmyslu (ale trpí silnou deaktivací), oxidační dehydrogenace dosud nebyla průmyslově implementována kvůli problému s nízkou selektivitou dostupných katalyzátorů v důsledku nadměrné oxidace produktů.

V poslední době nosné alkalické chloridy a hexagonální nitrid boru vykazují vysokou aktivitu a selektivitu při oxidační dehydrogenaci lehkých alkanů. Pro přímou dehydrogenaci lehkých alkanů jsou považovány za aktivní nanesené nanočástice ušlechtilých kovů. Je však zapotřebí podrobného zkoumání vztahu struktura-aktivita-stabilita pro jejich použití v reakci. Tato práce se zaměřuje na studium katalytického chování těchto tří slibných katalytických skupin pro (oxidativní) dehydrogenaci lehkých alkanů a pochopení jevů, které by mohly ovlivnit jejich aktivitu. V této práci byly zkoumány kritické parametry jako chemické složení, krystalinita, texturní vlastnosti, reakční podmínky, efekt předúpravy/regenerace, stabilita, katalytická aktivita a selektivita katalyzátorů při výrobě olefinů prostřednictvím (oxidativní) dehydrogenace alkanů. Byly charakterizovány čerstvé, ale i použité katalyzátory, aby se prozkoumaly fyzikálně-chemické změny, ke kterým došlo během reakce.

Při studiu chloridů alkalických kovů na nosiči bylo zjištěno, že vysoký výtěžek produkce olefinů, který je způsoben roztavenou vrstvou směsných solí vytvořených při reakční teplotě, je omezen deaktivací. Komplexní charakterizace poskytla vhled do mechanismu deaktivace a odhalila, že ztráta chloru v některých formách chlorovaných uhlovodíků způsobuje deaktivaci katalyzátoru.

S ohledem na nanesené nanočástice ušlechtilého kovu existuje několik různých metod pro zapouzdření kovových nanočástic. Jedním z nedávných přístupů je technika opětovného sestavení organizace shromáždění a demontáže, známá jako ADOR. V tomto výzkumu byla použita metoda ADOR k zapouzdření nanočástic Pd v zeolitech IPC-2 a IPC-4. Ukázalo se, že vrstvené zeolity s tenkými vrstvami, jako je UTL, nejsou vhodnými podporami pro zadržení kovových nanočástic, protože zeolitová kostra nemůže tolerovat těžké podmínky cyklické dehydrogenační reakce a regenerace. Nicméně zadržování

kovových nanočástic je účinný způsob, jak zabránit slinování a zlepšit katalytickou aktivitu nanočástic na nosiči ve srovnání s konvenční impregnací. Proto může toto omezení vést k lepší stabilitě v zeolitických strukturách, které mají silnější vrstvy.

Nový slibný nekovový katalyzátor, hexagonální nitrid boru, byl systematicky studován při oxidační dehydrogenaci propanu, aby bylo možné lépe porozumět skutečnému mechanismu a jevům zahrnutým v tomto komplikovaném systému. Tento katalyzátor vykazoval vysokou aktivitu a selektivitu, která byla doprovázena produkcí ethenu jako cenného vedlejšího produktu, spolu s nízkou oxidací produktů směrem k oxidům uhlíku. Přestože katalyzátory během reakce procházejí podstatnými změnami v chemickém složení, texturních vlastnostech a krystalinitě, aktivita a selektivita zůstávají téměř konstantní. Na rozdíl od předchozích studií, které uváděly obsah kyslíku jako hlavní faktor, v této práci se ukazuje, že reakce je řízena převážně chemií v plynné fázi. Proto je delší doba setrvání ve větším volném prostoru nezbytná pro tvorbu a šíření radikálů pro zlepšení produktivity, zatímco obsah kyslíku nehraje klíčovou roli. Ve skutečnosti je změna obsahu kyslíku výsledkem tvorby radikálů a nikoli příčinou. Tento katalyzátor je výsadní, protože se účastní spřaženého povrchově zprostředkovaného mechanismu plynné fáze, což vede k vyšší aktivitě a produktivitě ve srovnání s tradičními kovovými katalyzátory při oxidační dehydrogenaci lehkých alkanů trpících nadměrnou oxidací a nízkou selektivitou. Zdá se, že jednou ze skutečných rolí h-BN je ukončit generované radikály nebo adsorpci vody, které se tvoří v plynné fázi, za vzniku produktů nebo možná generování in situ okysličených látek, které nakonec vedou k tvorbě produktů. Předpokládá se, že v tomto systému je iniciační stupeň v plynné fázi a ne na povrchu katalyzátoru.

Klíčová slova

Oxidativní dehydrogenace, přímá dehydrogenace, heterogenní katalyzátor, lehký alkan, lehký olefin, charakterizace.

LIST OF PUBLICATION

Paper I:

Mehran Sajad, Oxidative dehydrogenation of propane over the boron-nitride catalysts, Scientific Papers of the University of Pardubice, Series A; Faculty of Chemical Technology, 26 (2020) 195–210.

Paper II:

Mehran Sajad, Roman Bulánek and Stanislav Šlang, Physico-Chemical Changes in the KCl-$MgCl_2$/La-FAU Composite Catalyst Induced by Oxidative Dehydrogenation of Ethane, Catalysts, 2021, 11 (3), 392. (IF: 3.9, Q2)

Paper III:

Yuyan Zhang, Ang Li, **Mehran Sajad**, Katarína Fulajtarová, Michal Mazur, Martin Kubů, Mariya Shamzhy, Milan Hronec, Roman Bulánek, Jiří Čejka, Imidazolium-type ionic liquid-assisted formation of the MFI zeolite loaded with metal nanoparticles for hydrogenation reactions, Chemical Engineering Journal, 412 (2021), 128599. (IF: 15.1, Q1)

Paper IV:

Mehran Sajad, Yuyan Zhang, Martin Kubů, Michal Mazur, Roman Bulánek, Jiří Čejka, Direct dehydrogenation of propane over Pd nanoparticles encapsulated within IPC zeolites with tunable pore sizes, Applied Materials Today, 29 (2022), 101644. (IF: 8.3, Q1)

Paper V:

Mehran Sajad, Roman Bulánek, Stanislav Šlang, Effect of the catalytic reactor arrangement and catalyst treatment in oxidative dehydrogenation of propane performance over hexagonal boron nitride, will be submitted in “Reaction Chemistry & Engineering”, (IF: 3.9, Q1)

LIST OF ABBREVIATIONS

Abbreviation	Meaning
ADOR	Assembly, disassembly, organization, reassembly
BET	Brunauer-Emmett-Teller
BNNT	Boron nitride nanotube
BN-OH	Hydroxylated boron nitride
COD	Crystallography open database
DDHP	Direct dehydrogenation of propane
DFT	Density functional theory
DH	Direct dehydrogenation
DRIFT	Diffuse reflectance infrared Fourier transform spectroscopy
EDS	Energy dispersive x-ray spectroscopy
FCC	Fluid catalytic cracking
FID	Flame ionization detector
FTIR	Fourier-transform infrared spectroscopy
hBN	Hexagonal boron nitride
ID	Internal diameter
ImILs	Imidazolium type ionic liquids
MS	Mass spectroscopy
NPs	Nanoparticles
ODH	Oxidative dehydrogenation
ODHE	Oxidative dehydrogenation of ethane
ODHP	Oxidative dehydrogenation of propane
RM	Reaction mixture
SC	Steam cracking
STEM	Scanning transmission electron microscopy
SVUV-PIMS	Synchrotron radiation vacuum ultraviolet photoionization mass spectroscopy
TCD	Thermal conductivity detector
TOF	Turnover frequency
TOS	Time on stream
XPS	X-ray photoelectron microscopy
XRD	X-ray diffraction

TABLE OF CONTENTS

INTRODUCTION

Light olefins are one of the most essential feedstocks for a variety of chemical industries around the world. Some examples are the synthesis of polymers (e.g., polyethylene and polypropylene), and oxygenates (e.g., ethylene glycol, acetaldehyde, acetone, and propylene oxide), which are involved in packaging, manufacturing, construction materials, etc., while the global demand for them is continually growing every year [1-3]. These olefins are traditionally produced by petroleum-derived steam cracking (SC) and fluid catalytic cracking (FCC), which are considered highly energy-intensive methods along with low selectivity and significant CO_2 emission. In such a harsh condition, generation of side products (alkanes) is unavoidable, and hence, preventing the wasting of valuable compounds is crucial. Moreover, current processes cannot meet the rapid global demand [1, 4]. Recently, the use of natural gas has become advantageous due to the depletion of fossil fuels and the abundant resources of shale gas explored around the world [5]. Therefore, the development of direct processes by means of catalysts is an interesting field for academic and industrial researchers, as catalysts are able to selectively produce the desired products, minimize the side reactions, avoid undesired environmentally harmful products, decrease the reaction temperature, and suppress the required energy consumption.

This thesis focuses on gaining deeper insight into catalytic systems for the selective production of light olefins such as ethene and propene from natural gas and their behavior. In this work, different types of catalytic systems were studied to gain a deeper understanding of the relationship between catalytic performance and its properties, and to find ways how to improve properties of these catalytic systems.

The parameters that have been considered are based on the type of the reaction (direct nonoxidative and oxidative dehydrogenation), the nature of the catalyst (metal and nonmetal catalysts), and the catalyst support. For this purpose, supported alkali chlorides, supported noble metals, and boron nitride have been studied. The behavior of each system including the catalytic activity, physicochemical changes before and after the reaction, and stability were investigated. Lastly, the advantages and disadvantages of individual systems were investigated, and different parameters that could have had an influence on the dehydrogenation reaction were studied.

1. STATE OF ART

1.1. Direct dehydrogenation

Direct dehydrogenation (DH) of light alkanes (C_nH_{2n+2} $C_nH_{2n} + H_2$) is an endothermic reaction that requires 113-134 kJ/mol to remove two hydrogen from the alkanes depending on the length of the chain. This reaction is equilibrium limited and takes place at relatively high temperatures; however, catalysts are able to decrease the temperature and provide adequate conversion and selectivity towards the desired products. The catalysts most commercially used in industry for the direct dehydrogenation of lower alkanes are based on platinum or chromium and usually necessitate high temperatures (550 to 750 ° C). These metals exhibited satisfactory ability to activate the C-H bond while avoiding C-C bond breaking, but apart from required high temperature, sintering and coke formation are inevitable challenge that cause catalyst deactivation [3, 6].

1.1.1 Supported metal nanoparticles

Recently, the use of supported metal nanoparticles (NPs) has been growing due to a better accessibility of the active sites for the feed molecules because the NPs are distributed on a support with a large surface area and subsequently lead to a higher efficiency for the chemical interactions. Furthermore, besides the improved accessibility of metals in these systems, a lower amount of metals is required, which is another reason for the high interest shown by researchers, specifically in the case of noble metals [7]. Hence, using supported noble metal particles is worth trying in the dehydrogenation of light alkanes, as this reaction has been reported to be structure-sensitive (geometric and electronic effect). For instance, intrinsic activity and selectivity of Pt NPs (Pt/Al_2O_3) in propane DH is dependent on their size and vary not in a same way. Smaller Pt particle size result in higher turnover frequency (TOF), but high selectivity and stability are achieved when the particle size is either lower than 1 nm or higher than 3 nm [8]. Also stability is connected with particle size, Campbell et al. reported that thermal stability of different metal species dramatically increased with increasing the particle size from 1 to 6 nm [9, 10]. They also showed that stability of smaller particle (Ag, 2-3 nm) could be preserved by strong bonding to the support, for instance oxygen vacancies in metal oxide supports can provide such strong bonding [11]. Furthermore, the nature of the support and the metal-support interaction will influence the shape, stability and atomic structure of the metallic nanoparticles [12]. Sitja et al. have shown that there is transition point from nonmetallic to metallic properties for Pd and Au around 2 nm. The particles larger than 1.8 nm exhibited a gradual increase in CO adsorption energy with increase in particle size, whereas for the particles below 2 nm there is an irregular oscillation, as the geometric and electronic structure of metal clusters significantly depends on the atomicity [13-15]. When such a small molecule is adsorbed on metal species, there will be also a geometric

deformation which would be dependent on the particle size again. It was reported that a considerable relaxation of Pt-Pt occurs when H_2 or CO are adsorbed on Pt nanoparticles of 1 nm size due to orbital hybridization. But when the size is increased, this adsorbate induced lattice relaxation of Pt nanoparticles is much smaller because of lower number of surface unsaturated Pt atoms [16]. As a result of this interaction effect between metal nanoparticles and the adsorbate molecule, the metal species could go through a dynamic transformation. It has been found that in oxidative atmosphere, Pd nanoparticles transform to smaller particles while after reductive treatment, Pd nanoparticles agglomerate into larger particles [17]. Thus, consecutive treatment that can provides such dynamic structural transformation, assist for the regeneration of deactivated catalysts.

Considering all, the stabilization of NPs against sintering and agglomeration under the severe condition of the dehydrogenation reaction is critical [18], and confinement of the metal NPs within zeolites is helpful solution for stabilizing the supported NPs. The unique properties of zeolites (e.g., crystallinity, ion exchange capacity, tunable porosity, acidity, high surface area, etc.) have enabled metal NPs to be confined in some cavities, layers, pores, or even exact locations inside the zeolite framework. The confinement of NPs within zeolites has shown considerable influence on the activity and stability of NPs compared to their impregnated counterparts, depending on the particle size and electronic construction of the NPs and the zeolite type and their interaction [12, 18-21]. The encapsulation of metals could be done by various approaches, such as post modification strategy (impregnation, Ion-exchange followed by post-treatment, template-guidance approach), and in-situ encapsulation strategy (in-situ hydrothermal synthesis, interzeolite transformation), etc [18]. In general, there are many variables capable of influencing the catalytic behavior of supported metal systems, such as size and shape of the metal nanoparticles, the nature of the support, the interaction between support and the metal nanoparticles, the presence of other metals, etc.

1.2. Oxidative dehydrogenation

Unlike direct dehydrogenation, oxidative dehydrogenation (ODH) of light alkanes ($C_nH_{2n+2} + ½\ O_2 \rightarrow C_nH_{2n} + H_2O$) is an exothermic and non-equilibrium limited reaction (-105 and -117 kJ/mol for ethane and propane, respectively) that requires an oxidizing agent and usually takes place at a lower reaction temperature (450-550 ˚C). However, after more than three decades of research on ODH, a suitable catalyst has not yet been reported to be interesting for industrial implementation. Transition metals, specifically vanadium, have attracted some attention during the last two decades, but the main problems were found to be poor selectivity, overoxidation to CO_2, and coke formation [2, 6, 22]. Nevertheless, interesting activity and selectivity have been reported for supported alkali and alkaline earth chlorides, as well as non-metallic catalysts, which are discussed in the following subsection.

1.2.1 Alkali and alkaline earth chlorides catalysts

Alkali and alkaline earth metal chlorides impregnated on various supports have been reported with encouraging activity and selectivity in the ODH of light alkanes. These modified catalysts exhibited higher activity and selectivity compared to chloride-free catalysts [22, 23]. The addition of mixed chlorides mainly affects the surface structure of the catalyst which means modification of the active centers. Usually, the reaction temperature is higher than the melting point of the eutectic composition of the salts; therefore, in these systems the molten salt layer plays a crucial role as the interface between the solid and gas phases, which is an advantage due to the possibility of working in a wide range of temperature, however these systems become more complicated because the interactions involved are in three phases. Furthermore, it was proposed that a gas-phase radical reaction occurred during the process due to the radical species generated by assistance of chlorine, but the inherent mechanism of chloride-modified catalysts is still the subject of debate [24-32]. Perez-Ramirez et al. showed the vital role of oxyhalogenation by generation of intermediates that could easily convert to valuable olefins. The high electron affinity of halogens for the hydrogen abstraction from hydrocarbons makes them suitable to be used in ODH. This affinity decreases in the order of Cl > F > Br > I [24]. In another work they showed oxychlorination led to higher olefin productivity compared to the oxybromination over europium oxychloride and europium oxybromide catalysts respectively [33].

There are two main reported reasons for such a high productivity for supported alkali chlorides systems. First, the dynamically rearranging molten interface which create or modify the active centers [22, 25, 27, 34, 35], and second, the hypochlorite species (OCl^-) that have often been hypothesized as the active site on the surface of the overlayer in these systems and as the reason for their observed higher activity and selectivity in the ODH reaction [25, 27, 30, 31, 36]. Lercher et al. proposed a mechanism based on their studied system ($LiCl/MgO/Dy_2O_3$), that includes dissolving of oxygen in the molten salt, which results in generation of OCl^- as the active species, then oxygen radical and chlorine radical are formed via OCl^- decomposition, whereas both are able to activate the alkane by hydrogen abstraction. Finally, the alkane radicals react with OH to form alkene and water. The reaction productivity is limited by chlorine concentration and diffusion strains through the molten salt interface [29].

The molten layer as a dynamic interface plays a crucial role in selectivity by facilitating the desorption of olefins. It was shown that ethene is more stable via adsorption at the interface than dissolving in liquid chloride. Moreover, the carbon floats on the surface of molten layer and could be skimmed off easily rather than coke formation [27, 30, 31, 34, 35].

In one of the most promising reports, the study of supported binary alkali and alkaline earth chlorides exhibited 100% selectivity toward ethylene at 40% ethane conversion which seems to be a potential

candidate for future industry [23]. In this report a new catalyst system for activating ethane at very low temperatures was shown, but unfortunately, more detailed characterization of the materials or information on the stability of those systems were not included.

But according to the reports, the unstable behavior is a drawback and reasons depend on the nature of the salts and supports [26, 31, 35, 37-41]. Generally, different pathways of chlorine loss have been considered as the main cause of deactivation [26, 35, 37]. For instance, in metal oxide supports, the interaction between support and chlorine or water and chlorine results in formation of HCl over time and cause deactivation [31, 42]. Also chemical phase transformation during the reaction is one another reported origin [26]. As it is difficult to prevent HCl intermediate from scaping at high temperature, addition of chlorinated compound was suggested for the regeneration [36, 37, 41]. Also, presence of HCl gaseous feed during the reaction was tried on CeO_2-based catalyst and exhibited significant improvement in the activity and selectivity of this system in ODH of ethane [43].

Therefore, investigation of finding an efficient chlorine-promoted catalyst and studying of the deactivation mechanism could be a valuable research to find the way to industry in the future.

1.2.2 Boron nitride

One promising candidate for the nonmetallic group of catalysts in ODH is hexagonal boron nitride (hBN), an analogue of graphite, which is relatively new compared to the others in the field of dehydrogenation[2]. In the past, boron nitride had been considered chemically inert and used as a catalyst diluent due to its high thermal stability and high thermal conductivity, which limits the formation of hot spots, making it appropriate for industrial applications [44]. Firstly, in 2016, Hermans et al. [45] reported their observation about the activity and selectivity of hexagonal boron nitride and boron nitride nanotube (BNNT) for propane ODH which were higher than traditional transition metal catalysts (for e.g. V/SiO_2) and unlike traditional catalysts that produce CO_x as an unavoidable side product, the main side product in this system was ethene which is obviously much more valuable. At the beginning, it was hypothesized that the armchair edges contain B-O-O-N are the active site [45]. Edge-hydroxylated boron nitride (BN-OH) was reported afterward to have a higher activity than any other catalyst at that time, and it was also stable. Density functional theory (DFT) calculations showed that the formation of B-O-B bridges after the dehydration of adjacent B-OH is the key point and is reversible by gaseous water [46]. This idea was clearly in disagreement with the first hypothesis. Since then, there has been a high interest in studying this system and investigating the active site and mechanism. Soon, the first hypothesis about the armchair edges with B-O-O-N structure was invalidated because the catalysts without nitrogen also showed similar activity, and it was concluded that boron is the key element [47]. In that research, a range of metal borides were tested, including NiB, HfB_2, B_4C, TiB_2, WB, hBN, and elemental boron. These primary results and reports led to the conclusion that

boron is oxidized to boron oxide (BO_x) and acts as an essential active site, and the catalytic activity depends on the concentration of boron at the surface [48]. Shi et al. reported a comparison between traditional catalysts and promising boron catalyst for dehydrogenation [49]. Selectivity toward CO_2, oxygen and alkane reaction order, side products, active sites, and reaction mechanisms were the key points. The negligible selectivity of CO_2 and the long-lasting stable productivity of the boron catalyst make it highly promising for industrial implementation. The presence of oxygen and its role were also discussed, and since it showed a reaction order of 0.5, it suggests the importance of dissociative adsorption of oxygen. Furthermore, unlike metal oxides that function without oxygen, hBN does not exhibit any activity in the absence of oxygen, which means that the active sites are formed under the reaction condition. In another work, it was also shown that the alkane partial pressure has a reaction order of 1 for metal oxides with the Mars-Van Krevelen mechanism, which is not the same as BN with a reaction order of 2 and without lattice oxygen [46], therefore, it is obvious that there are different mechanisms in the boron catalyst compared to the traditional supported metal oxide catalysts. As mentioned above, a valuable side product by using hBN is ethene, meaning that the methyl group formed by the C-C bond cleavage takes different reaction pathways. They can generate C_2H_4 by oxidative coupling that results in better selectivity of C_2 products [50]. Although in situ boron oxide species formation has been hypothesized to be crucial , in the meantime, gas-phase reactions are intensely involved. [51, 52] However, the nature of active sites and the exact mechanisms still need to be unveiled. The first experimental evidence of the gas-phase reaction was the detection of methyl radicals by using synchrotron radiation vacuum ultraviolet photoionization mass spectroscopy (SVUV-PIMS) [52]. The presence of the gas phase radical agrees with the kinetic data on C_2 as the main side product and shows that the methyl radicals contribute to the formation of the C_1 and C_2 products. Surprisingly, no propyl radicals were detected, suggesting that propene is generated via a surface-controlled pathway. Nevertheless, Venegas et al. [53] claimed that if propene formation were surface controlled, the catalytic behavior and selectivity would not be different from vanadium-based catalysts; therefore, they hypothesized that propyl radicals react with $HOO^{\bullet}$ radicals in the gas phase. This is in direct disagreement with the first report using SVUV-PIMS without detection of propyl radicals. Later, a study of reactor parameters revealed that the change in catalyst mass, reactor diameter, and catalyst dilution resulted in the importance of the gas phase reaction as the main driver and the catalyst surface as the initiator [54]. Recent theoretical studies suggest two approaches regarding how to explain the high activity and selectivity of hBN; first, by detached nano-sized boron oxide clusters that diffuse with the gas flow, and subsequently, the tricoordinated boron site dehydrogenates the alkane. B-O-B sites are claimed to be more reactive than B-OH groups in eliminating alkoxyl radicals in the ODH of light alkanes, and the edge boron sites (B-OH) can activate atmospheric dioxygen [55]. The second is about in situ generation of surface boron peroxo species at the B-O-B sites that acts as a mild oxidant and prefer secondary hydrogen over the primary hydrogen, and thus

increases the selectivity by preventing over oxidation [56]. Lastly, a comprehensive study using the operando spectroscopy technique in combination with theoretical calculations detected the presence of short-lived intermediates such as radicals and oxygenates, and concluded that boron peroxo-like species on the surface are responsible for propane activation while radicals are derived from BO dangling sites; after desorption of radicals and oxygenates, gas-phase H-abstraction chemistry will be initiated [57].

Based on this chapter, boron nitride and in general, boron-based catalysts, are highly promising in the field of dehydrogenation but understanding the nature of actual active species and the mechanisms involved during the ODH reaction is still a challenge for researchers and future industrial applications.

2. AIMS AND SCOPE OF RESEARCH

All in all, in the targeted research field of this dissertation thesis (conversion of light alkanes to alkenes), there are still many ambiguous points that are potentially helpful to take the catalysts out of the lab and finally put them into the industry. Therefore, we have tried here to shed light on some of those points. These are included the following questions:

- Is the high activity and selectivity of the supported alkali chlorides stable? And if not, what is the cause?
- How does the encapsulation of noble metal NPs affect their catalytic activity and stability in the dehydrogenation of light alkanes?
- What is the mystery of hBN exceptional productivity in oxidative dehydrogenation of light alkanes?

To address these questions and meet the objectives of the thesis, the following actions were taken:

- Synthesis of some of the most active and selective supported alkali chlorides catalyst, measurement of catalytic activity in ODH of light alkanes. Comprehensive characterization of the fresh and spent catalysts, and identification of the side products and clarifications of the possible deactivation.
- Confinement of noble-metal NPs within various zeolites in collaboration with colleagues at the Faculty of Sciences, Charles University, Prague. Investigation of the catalytic activity and selectivity in dehydrogenation of light alkanes. Cyclic catalytic tests for studying the stability and regeneration capability of the catalysts. Comprehensive characterization of the fresh and spent catalysts, and investigation of the catalyst behavior.
- Studying hBN behavior in oxidative dehydrogenation of light alkanes, including wide range of catalytic test conditions and comprehensive characterization of all the fresh and spent catalysts. Investigation of physicochemical changes on hBN under different reaction atmospheres, time on stream, different pretreatments, total flowrates, temperatures, reactor geometry, catalyst mass, etc., to discover the influence of effective parameters on the catalytic activity. Understanding the role of catalyst based on the obtained results from designed experiments and theoretical studies.

3. EXPERIMENTAL

3.1. Materials

The list of used chemicals in this work are listed in Table 1.

Table 1. List of chemicals

Name	Formula	specification	Supplier
Ammonium Faujasite	NH_4-FAU	Si/Al = 2.55	Zeolyst
boric acid	H_3BO_3	99.5 % purity	Sigma-Aldrich
Ethane	C_2H_6	99.5% purity	Linde
Helium	He	99. 996% purity	AIRPRODUCTS
Hexagonal boron nitride	hBN	98% purity, 1 um particle size	Sigma-Aldrich
Lanthanum (III) chloride heptahydrate	$LaCl_3.7H_2O$	99.999 % purity	Sigma-Aldrich
Magnesium dichloride	$MgCl_2$	99.9 % purity	Sigma-Aldrich
Nitrogen	N_2	99.999 purity	AIRPRODUCTS
Oxygen	O_2	100% purity	AIRPRODUCTS
Potassium chloride	KCl	99.5 % purity	Sigma-Aldrich
Propane	C_3H_8	99.5% purity	Linde

3.2. Experiments and characterization

3.2.1 Supported alkali and alkaline earth chlorides

To investigate the stability of highly active and selective supported alkali chloride, it was necessary to prepare the catalyst support by solid-state ion exchange of NH_4-FAU zeolite with $LaCl_3.7H_2O$. The precursors were mechanically mixed and then heated in an atmosphere control furnace at 500 °C for 12 hours under N_2 flow. After that, extensive mixing of KCl and $MgCl_2$ with La-FAU produced the prepared catalyst. The mechanical mixture was converted to fresh catalyst just before the catalytic test during pretreatment in the flow of helium at 500 °C. The catalytic behavior of the prepared catalyst was then investigated in oxidative dehydrogenation of ethane in a plug-flow fixed-bed tubular-shaped reactor, using desired mass of catalyst with a grain size of 0.35 to 0.50 mm at 500 ° C and under atmospheric pressure. The products were analyzed with an online gas chromatograph with a flame ionization detector (FID) and a thermal conductivity detector (TCD). The pretreatment, reaction mixture, total flow rate, blank experiment, and measurement condition details are declared in **Paper II**. As a deactivation trend was observed for this system, the next step was the characterization of the physical mixture, fresh and spent catalysts to study the physicochemical changes before and after the reaction. The analysis of the chemical composition was done by energy-dispersive X-ray spectroscopy (EDS) combined with SEM. In addition, X-ray diffraction (XRD) of spent catalyst was used for monitoring the changes in crystallinity and population of crystal phases. The

products of the ODHP reaction were analyzed by operando mass spectrometry in order to monitor side products of reaction. Furthermore, N_2 physisorption isotherms were used to see changes in textural properties of the physical mixture, fresh and spent catalysts.

3.2.2 Encapsulated Pd NPs within zeolite

The Pd NPs were encapsulated within MFI, IPC-2 and IPC-4 zeolites at the Charles University Center of Advanced Materials via two different approaches; first, using alkoxysilane functional imidazolium-type ionic liquids (ImILs) as assistant agents to protect metal precursors in Pd encapsulated within MFI (**paper III**). And in the second approach, well-dispersed Pd nanoparticles were encapsulated within IPC-2 and IPC-4 zeolites using the Assembly, Disassembly, Organization, and Reassembly (ADOR) process based on the 3D-2D-3D transformation of UTL zeolite (**paper IV**). To investigate the catalytic activity of the encapsulated Pd NPs, the catalysts were measured in direct dehydrogenation of propane in a plug flow fixed-bed tubular shape reactor, using the desired catalyst mass with a grain size of 0.35 to 0.50 mm at 600 °C and under atmospheric pressure. The products were analyzed with an online gas chromatograph with a flame ionization detector (FID) and a thermal conductivity detector (TCD). The pretreatment, reaction mixture, total flow rate, blank experiment, and measurements condition details are declared in **Papers III** and **IV**. A comparison was made between the catalysts by using the rate of propene formation per one gram of Pd in one second, which exhibited different activity of the catalysts, thus it was necessary to test if the catalysts are stable and, if not, how their behavior changes after regeneration, therefore, a cyclic test was designed to repeat the catalytic measurements four times, and after each measurement a regeneration step was done via treating the catalyst under an oxidative atmosphere at reaction temperature. Also, the intrinsic activity of the supported Pd NPs as turnover frequency was studied by considering the average particle size of Pd and assuming that only Pd atoms on the surface of the particles were involved in the reaction. The next step was to understand whether there is any connection between different catalytic results and the size of Pd NPs; therefore, scanning transmission electron microscopy (STEM) was used to show the Pd NP size and distribution before and after the reaction. The other characterization methods that helped to investigate what could possibly occur during the reaction were study of crystallinity by XRD patterns, textural properties by nitrogen physisorption isotherms, and availability of active sites through CO adsorption via collecting diffuse reflectance infrared Fourier transform (DRIFT) spectra through in situ measurements on a spectrometer equipped with a DRIFT cell.

3.2.3 hBN

The catalytic activity and stability of hBN in oxidative dehydrogenation of propane were measured in a plug-flow fixed-bed tubular shape reactor, using desired mass of the catalyst with the grain size of 0.35 to 0.50 mm at 490 °C under atmospheric pressure. Details of the pretreatment, the composition of the reaction

mixture, and measurement condition details are declared in **Paper I**. To investigate the physicochemical changes that occur during the reaction over hBN, the catalyst was treated under various conditions at the reaction temperature (490 °C), including treatment under different atmospheres for two hours (He, He/O_2, He/C_3H_8, $He/O_2/C_3H_8$, with the flow rates for He: 11, O_2: 3 and C_3H_8: 6 ml min^{-1}), different time on the stream (TOS) in the ODHP atmosphere ($He/O_2/C_3H_8$) from 15 minutes to 10 hours. The fresh and treated catalysts were characterized by XRD, nitrogen physisorption isotherms, Raman and infrared spectroscopy, and EDS to clarify the changes in crystallinity, textural properties, skeletal vibration, and chemical composition. To understand the role of boron oxide species in this catalytic system, the hBN catalyst was impregnated with boric acid for 5 wt.% via conventional impregnation. Boric acid was dissolved in water by stirring, and then hBN was added to the solution and continued stirring at 75 C until the solvent was evaporated. Then the powder obtained was dried at 110 ˚C over night and labeled as impregnated. Later, to measure the catalytic activity of the washed sample, the impregnated hBN was stirred for one hour in methanol, filtered and dried at 110 °C overnight and labeled as washed. Moreover, it was needed to compare the activity of the boron nitride with low specific surface area with another synthesized boron nitride with significantly larger specific surface area. Therefore, the high surface area sample was synthesized by colleagues in "Iran University of Science and Technology" by using guanidine carbonate and boric acid as precursors. After dissolving the precursors in water, the solvent was evaporated at 80 ˚C over night, and then the white powder was treated at 1000 ˚C under N_2 atmosphere.

On the other hand, to study the effect of gas phase reaction, a set of reactors with different total volume based on different inner diameter (id: 9, 10, 12.3, 14.5, 15.5 mm) were prepared and the catalytic activity of a similar mass of hBN was measured in all of them in the same condition. To investigate whether the gas-solid interface plays any role, a reactor with the same diameter as the largest reactor (id: 15.5 mm) with a lower height was prepared to provide the same void volume as the smallest reactor (id: 9 mm). Later, different mass of catalyst (50, 100, 150 mg), different total flow rate (15 to 35 ml min^{-1}) and effect of catalyst dilution (with SiC or quartz sand) were also examined to understand what is the main driver of the reaction.

To have a better knowledge of how coupled surface mediated and gas phase reactions are cooperatively involved, the generated products under the reaction condition were monitored in situ via a mass spectrometer. Also, the effect of oxygen presence was investigated by a pulse experiment dosing oxygen and monitoring the change in the detected propane through the mass spectrometer.

3.2.4 Calculations

For evaluating the catalyst activity, it is important to distinguish the overall performance of the catalyst and the intrinsic activity of the active sites. The overall performance includes the alkane conversion, selectivity to products, and products yield.

The alkane conversion was calculated using Equation 1.

$$X_a = \frac{n_i - n_t}{n_i} \times 100 \qquad \text{(Equation 1)}$$

Where X_a is the conversion of corresponding alkane (%), while n_i is the molar flow of corresponding alkane in inlet gas mixture (mol min^{-1}), and n_t is the molar flow of the alkane at the measured time-on-stream in outlet gas mixture (mol min^{-1}).

The selectivity toward products was calculated based on Equation 2.

$$S_x = \frac{n_x}{n_p} \times 100 \qquad \text{(Equation 2)}$$

Where S_x is the selectivity of product x (%), n_x is the number of alkane moles converted to product x (nmol), and n_p is the number of alkane moles converted to all products (nmol).

The yield was calculated using Equation 3.

$$Y_x = \frac{X_a \times S_x}{100} \qquad \text{(Equation 3)}$$

Where Y_x is the yield of product x (%), X_a is the conversion of corresponding alkane (%) base on Equation 1, and S_x is selectivity toward product x (%) according to the Equation 2.

Intrinsic activity of the active phase of catalysts was then expressed as the rate of propene formation over metal NPs mass unity using Equation 4 and turnover frequency that was calculated using Equation 5.

$$R_{alkene} = \frac{F_a \,.X_a \,.\, S_x}{m_{Pd}} \qquad \text{(Equation 4)}$$

Where R_{alkene} is the rate of alkene formation ($mmol_{alkene}\ s^{-1}\ g_{pd}^{-1}$), while F_a is the molar flow of corresponding alkane (mmol s^{-1}), X_a is the conversion of alkane (%), S_x is the selectivity towards alkene x (%) and m_{Pd} is the mass of Pd NPs (g).

$$TOF = \frac{F_a \,.\, X_a}{n_{Pd}} \qquad \text{(Equation 5)}$$

Where TOF is turnover frequency (s^{-1}), F_a is molar flow of the corresponding alkane (mol s^{-1}), X_a is the conversion of alkane (%), n_{Pd} is the surface Pd content (mol). The content of Pd surface atoms was obtained based on the Pd face-centered cubic lattice with a= 0.38907, where 2 Pd atoms are in the cube wall. Therefore, the surface density (D_s) is:

$$D_s = \frac{2}{0.38907^2} \approx 13.2 \text{ atoms per nm}^2 \quad \text{(Equation 6)}$$

And the number of atoms on the surface of the nanoparticle ($n_{Pd/S}$) is:

$$n_{Pd/S} = S_{Pd} \times D_s \quad \text{(Equation 7)}$$

Where S_{Pd} is the surface of the Pd NPs calculated from the average particle size obtained by STEM, and D_s is the surface density from equation 7.

Thus, the amount (mol) of Pd on the surface of the particle (n_{Pd}) is calculated by:

$$n_{Pd} = \frac{n_{Pd/S}}{N_A} \quad \text{(Equation 8)}$$

Where $n_{Pd/S}$ is number of Pd surface atoms from equation 7, and N_A is Avogadro number.

4. RESULTS AND DISCUSSION

This chapter is divided into three parts, based on the aims and the questions defined in the chapter 4 of this thesis. Each part discusses and summarizes the published data related to a specific catalyst and its behavior. The studied reactions are oxidative dehydrogenation of ethane (ODHE) by supported alkali chlorides, direct dehydrogenation of propane (DDHP) by supported metal NPs, and oxidative dehydrogenation of propane by boron nitride. Scheme 1 shows how these data are related to the topic of this dissertation thesis.

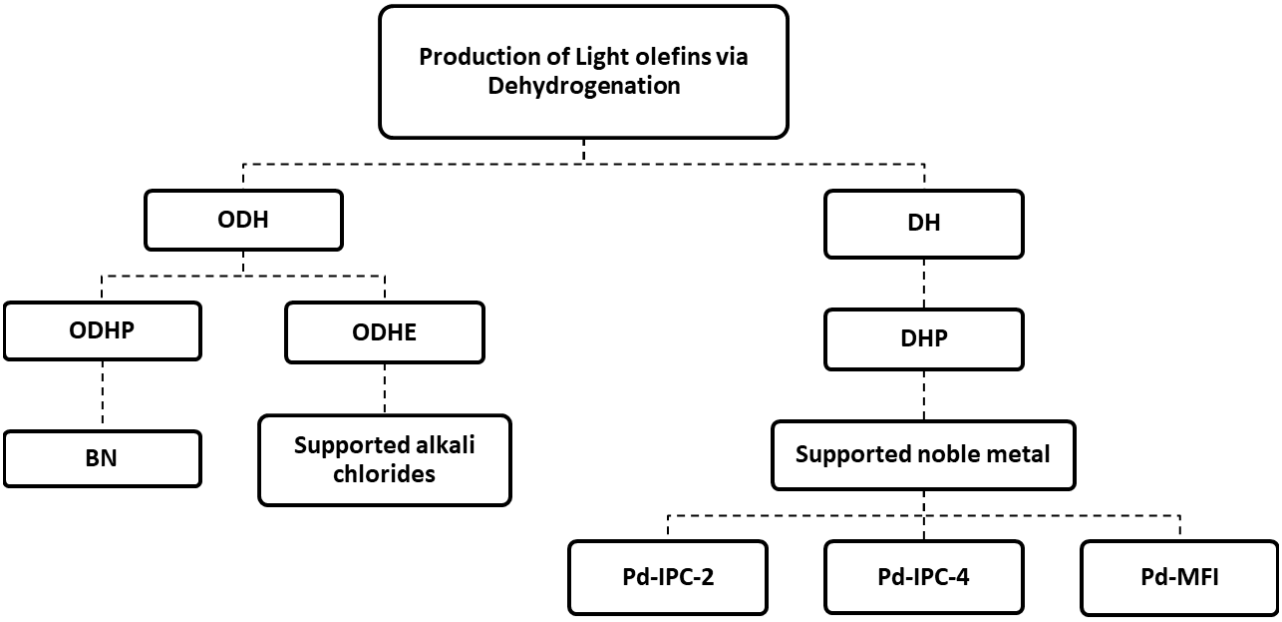

Scheme 1. The diagram on the relation between studied catalytic systems and the thesis topic.

4.1. Supported alkali and alkaline earth chlorides

In the first part of our research, a range of binary and ternary alkali and alkaline earth chlorides were prepared including KCl-$MgCl_2$/La-FAU, NaCl-$MgCl_2$/La-FAU, CsCl-$MgCl_2$/La-FAU, RbCl-$MgCl_2$/La-FAU, KCl-NaCl-$MgCl_2$/La-FAU and tested in the oxidative dehydrogenation of ethane. The catalytic activity of the FAU zeolite and La-FAU supports was measured too, that exhibited very low yield of ethene productivity. Among all the prepared catalysts, the KCl-$MgCl_2$/La-FAU exhibited the highest efficiency (57% yield) in ODH of ethane, therefore it was considered as the representative of this group and has been discussed in this section while more details could be found in **Paper II**. Also, a comparison between this system and similar reports in the literature has been shown in Table 2. In all cases, the addition of chlorides resulted in higher activity and selectivity, compared to the pristine support. However, the studied system in

this work is rather incomparable due to exhibiting high performance at low temperature that is critical for industrial applications. It is noteworthy that for the reports on higher yield of propene formation higher reaction temperature was applied in range of 550-750 ˚C.

The observed catalytic activity of KCl-$MgCl_2$/La-FAU was extraordinary, 80% conversion of ethane with 72% selectivity to ethene at 500 ˚C (Figure 1). Furthermore, a negligible amount of CO_2 and CH_4 was detected without any traces of CO (**Paper II**). This exceptionally low temperature activity was stable for a short time, then the ethane conversion decreased significantly and this is the fact that had not been described previously in the literature. Meanwhile the selectivity towards ethene increased slowly, but there were some side products that could not be identified by gas chromatography, as the column was designed to determine C_1-C_3 alkanes and alkenes, CO_X and O_2 (**Paper II**). Hence, it seemed that the identification of these products could help to find the reasons for the observed deactivation in this system, and it is discussed in the following section.

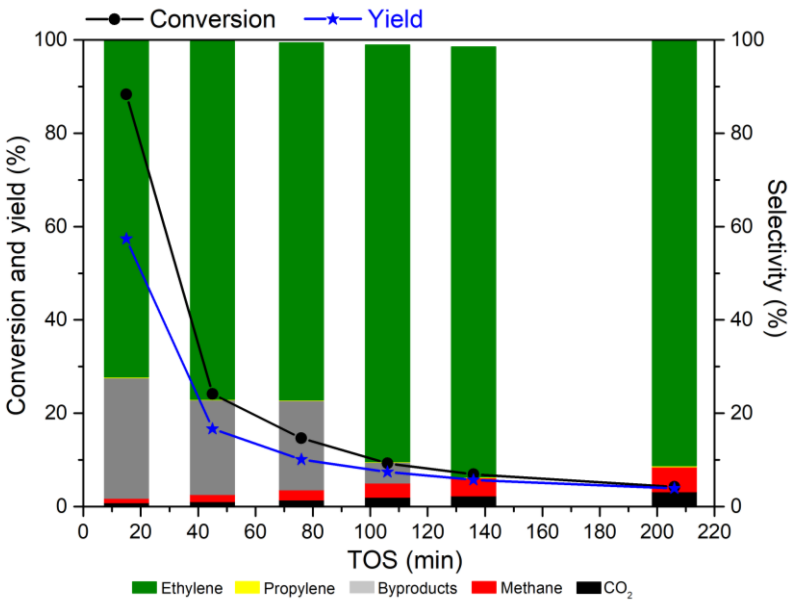

Figure 1. Catalytic activity and stability of KCl-$MgCl_2$/La-FAU in ODH of ethane as a function of time on stream.

Table 2. A comparison between similar reported study to this work.

Catalyst	Conversion (%)	selectivity (%)	Temperature (˚C)	Yield (%)	TOS (min.)	Ref.
KCl-$MgCl_2$/La-FAU	80	72	500	57	15	This work
NaY-La(Cl)-(NaMg)	2	100	500	2	-	[23]
NaY-La(Cl)-(KMg)	27	100	500	27	-	[23]
NaY-La(Cl)-(RbMg)	40	100	500	40	-	[23]
NaY-La(Cl)-(CsMg)	7	100	500	7	-	[23]
NaY-Binary(NaMg)	3	100	500	3	-	[23]
NaY-La(Cl)-(NaKMg)	20	100	500	20	-	[23]
LiCl/SiO_2	99	79	600	78	5	[26]
NaCl/SiO_2	88	69	550	61	5	[26]
KCl/SiO_2	70	75	550	52	5	[26]
LiCl/SZ (sulfated zirconia)	98	70	650	68	1	[38]
LiCl/AZ (amorphous zirconia)	87	60	650	52	1	[58]
LiCl/ZrON	95	71	650	68	1	[58]
LiCl/ZrOCl	28	97	650	27	1	[58]
LiCl/$ZrSO_4$	89	83	650	74	1	[58]
LiCl/ SZ (sulfated zirconia)	53	90	650	48	1	[59]
$BaCl_2$–TiO_2–SnO_2	66	93	720	60	30	[39]
Li/Dy/Mg/O/Cl	-	-	650	77	-	[29]
(Li-K)Cl-(Dy_2O_3/MgO) membrane	34	97	700	33	-	[27]
(Li-K)Cl-(Dy_2O_3/MgO) membrane	85	75	750	64	-	[27]
KCl-$MgCl_2$/La-FAU	22	77	500	17	45	This work
$PbBi_3O4Cl_3$	51	88	660	45	60	[37]
KCl-$MgCl_2$/La-FAU	8	89	500	7	106	This work
Li/K/Cl-MgO/Dy_2O_3	5	94	550	5	120	[35]
Li/Na/Cl-MgO/Dy_2O_3	2	75	500	2	120	[35]
Li/Cl-MgO/Dy_2O_3	2	60	500	1	120	[35]
K/Cl-MgO/Dy_2O_3	2	40	500	1	120	[35]
Na/Cl-MgO/Dy_2O_3	2	37	500	1	120	[35]
KCl-$MgCl_2$/La-FAU	4	91	500	4	206	This work
$SrBi_3O_4Cl_3$	20	89	660	17	360	[37]
$SrBi_3O_4Cl_3$ + $SrCl_2$	35	89	660	31	360	[37]
$SrBi_3O_4Cl_3$ + 2$SrCl_2$	44	90	660	39	360	[37]
$SrBi_3O_4Cl_3$ + KCl	36	96	660	34	360	[37]
$SrBi_3O_4Cl_3$ + $SrCl_2$ + KCl	45	92	660	42	360	[37]
$SrBi_3O_4Cl_3$ + $SrCl_2$ + LiCl	42	94	660	40	360	[37]
$SrBi_3O_4Cl_3$ + $SrCl_2$ + NaCl	41	95	660	39	360	[37]
LiCl/ SZ (sulfated zirconia)	70	66	650	46	900	[38]

The mass spectroscopy (MS) was found to be helpful technique for identifying unknown side products and resulted in finding chlorinated hydrocarbons include chloromethane, ethyl chloride, and chloroethene at the beginning of the reaction (Figure 2). Traces of HCl were also observed that probably act as an unstable intermediate. As time passed and the ethane conversion decreased, the nature of the side products changed (dashed area in Figure 3 and **Paper II**). The new side products consisted of some higher hydrocarbons (C_5) or oxygenates. These include allyl vinyl ether; 1,3-dimethylallene; trans-2-methyl-2-butenal; 2-methyl-2-butenal; 4-pentyne-2-ol; 3-butynoic acid; 2-buten-4-olide; 1-ethyl-2-methylacetylene; and 3-methyl-2-butenal.

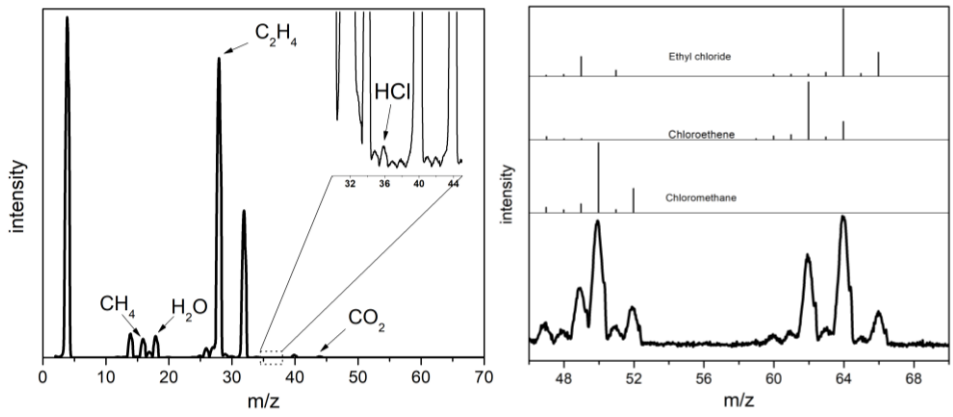

Figure 2. Mass spectrum of the products of the ethane ODH over KCl-$MgCl_2$/La-FAU (left), and details of low-intensity signals at m/z 46–70 compared to the model spectra of the three most probable chlorinated compounds formed during the reaction.

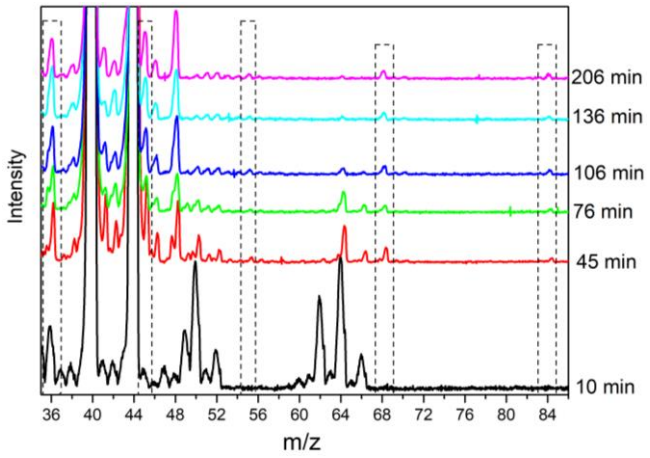

Figure 3. Mass spectra of the side products of ethane ODH over KCl-$MgCl_2$/La-FAU during the reaction time. The changes in side products over time are indicated by dashed area.

The changes in the chemical composition of the catalyst were tracked by EDS. It was disclosed that the content of alkali and alkaline earth metals remained almost constant for the time under the reaction stream. Meanwhile, the chlorine content had been continuously reduced and finally leveled off by 75% loss of

chlorine which agrees with the observation by mass spectroscopy and formation of chlorinated side products. The 25% remaining were probably inaccessible from the surface to escape or bounded to more stable compounds (**Paper II** and Table 3).

Table 3. Chemical composition of KCl-$MgCl_2$/La-FAU catalyst measured by EDS based on the atomic percentage of elements.

		Spent catalysts, different TOS (min.)				
Element	**Fresh**	**15**	**45**	**76**	**136**	**223**
O	52.7	57.8	57.6	56.3	57.6	60.0
Na	0.7	0.9	0.9	0.7	0.7	0.7
Mg	9.4	11.6	10.4	13.1	13.2	9.7
Al	3.9	4.4	4.5	4.2	4.0	4.3
Si	9.1	11.1	11.4	10.8	10.4	11.8
Cl	11.5	11.1	7.6	7.1	6.6	6.3
K	5.8	5.5	5.2	5.4	5.1	5.4
La	1.7	2.6	2.5	2.4	2.5	1.9

The XRD patterns revealed that after the treatment at temperature higher than the eutectic point, a solid solution of chlorides was formed because of the dissolution of chlorides in each other (Figure 4). The presence of FAU, LaOCl, and KCl was evidenced before and after the heat treatment, which showed their stability. It is noteworthy that the presence of La in LaOCl means that not all of the lanthanum was in the cationic sites of zeolite. Furthermore, not any form of $MgCl_2$ was detected after the formation of the molten layer that discloses its lability. After the reaction alongside LaOCl and KCl, more crystalline phases were presented, for instance, SiO_2 and MgO. In the case of MgO, it shows that after chlorine loss during the reaction, its crystallinity changed to a different phase by taking advantage of oxygen as a substitution. More details about changes in crystalline phases, and also the textural properties are discussed in **Paper II**.

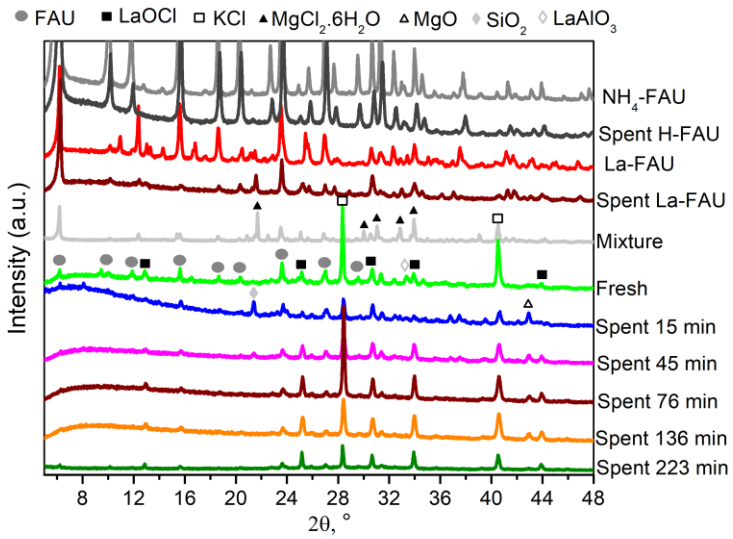

Figure 4. The X-ray diffraction patterns of the support, physical mixture and the catalyst before and after the reaction.

According to this chapter, it could be concluded that the supported alkali and alkaline earth chlorides are highly active and selective in ODH of ethane at fairly low temperature, but not stable enough for long term use to be applicable in the near future. These systems need modification to prevent chlorine loss which cause the deactivation by formation of side products such as chlorinated hydrocarbons, higher hydrocarbons and oxygenates. One option to solve this problem is to dose chlorine gas into the reaction mixture, as in the case of the LiCl/MgO catalyst for oxychlorination, but this would promote the formation of chlorinated hydrocarbons and a corrosive environment

4.2. Supported metal NPs

The confinement of metal nanoparticles within zeolite matrices has garnered significant attention because of its potential applications in catalysis, adsorption, etc. Zeolites, possessing a well-defined porous structure and high thermal stability, offer an ideal environment for the encapsulation and stabilization of metal nanoparticles. This confinement effect can lead to enhanced catalytic properties, such as improved selectivity, increased activity, and a prolonged catalyst lifetime. The interactions between the metal nanoparticles and the zeolite framework play a crucial role in determining the size, distribution, and accessibility of the encapsulated nanoparticles. Understanding the confinement effects at the atomic and molecular levels is of paramount importance for designing novel catalysts with tailored properties. This dissertation aims to investigate the influence of metal nanoparticles confinement within zeolites on catalytic activity, by utilizing advanced characterization techniques to unravel the intricate interplay between the metal nanoparticles and the zeolite framework, and ultimately providing insights for the development of highly efficient catalytic systems. To meet this goal, structures such as MFI, IPC-2 and IPC-4 zeolites were chosen to be tested for Pd NP confinement. For each support, a different method of encapsulation was utilized and an impregnated sample was synthesized by the conventional impregnation method to compare the results.

The Pd NPs were encapsulated within MFI zeolite via a new method by using alkoxysilane functional imidazolium-type ionic liquids (ImILs) as assistant agents to protect the metal precursor against precipitation during the hydrothermal synthesis of the MFI zeolite. The final encapsulated catalyst is labeled as Pd@MFI in this thesis (Pd@MFI_ImILs in **paper III**), and the impregnated catalyst was labeled as Pd/MFI in this thesis (Pd@MFI_Imp in **paper III**).

In the case of IPC-2 and IPC-4 zeolites, the Assembly, Disassembly, Organization, and Reassembly (ADOR) process was used based on the 3D-2D-3D transformation. IPC-2 and IPC-4 zeolites were prepared from an IPC-1P precursor derived from hydrolysis of UTL zeolite using the ADOR approach to encapsulate Pd NPs inside the zeolitic layers (**Paper IV**).

Then the catalytic activity of Pd NPs encapsulated within MFI, IPC-2, and IPC-4 zeolites in direct dehydrogenation of propane was studied and compared to their impregnated counterparts. Interestingly, all encapsulated catalysts exhibited higher rate of propene formation compared to impregnated catalysts (Figure 5). There are several factors involved in the higher activity of the encapsulated catalysts, such as the uniformity of the distribution of Pd NPs within the zeolitic support in the encapsulated catalysts. Also, the size of Pd NPs plays a crucial role, as the smaller NPs provide a higher specific surface area, but in the impregnated samples, the metal NPs form larger sizes, which are not uniformly spread. The STEM images of the encapsulated catalysts exhibited a homogeneous distribution of Pd NPs with a narrow size distribution that shows the successful confinement of the metal NPs within the zeolite. Furthermore, the impregnated samples showed an uneven distribution of Pd NPs with significantly larger particle sizes, which were placed mainly on the external surface of the zeolite crystals (**Paper III, IV,** and Figure 7 and Figure 8). Another effective parameter is the different intrinsic capacity of metal NPs with different arrangements. The electronic structure made by the connection between Pd atoms and the support is potentially one of the most important sources of higher capability of the encapsulated catalysts to catalyze the dehydrogenation reaction in these systems (**Paper III, IV**). The Pd@IPC-2 and Pd@IPC-4 showed higher activity than Pd@MFI, which could be connected to the zeolite structure, and also the aluminosilicate nature of MFI compared to the siliceous nature of IPC zeolites. These parameters will be discussed later in this chapter. It should be mentioned that the activity of Pd@MFI catalyst in DH reaction has not published yet.

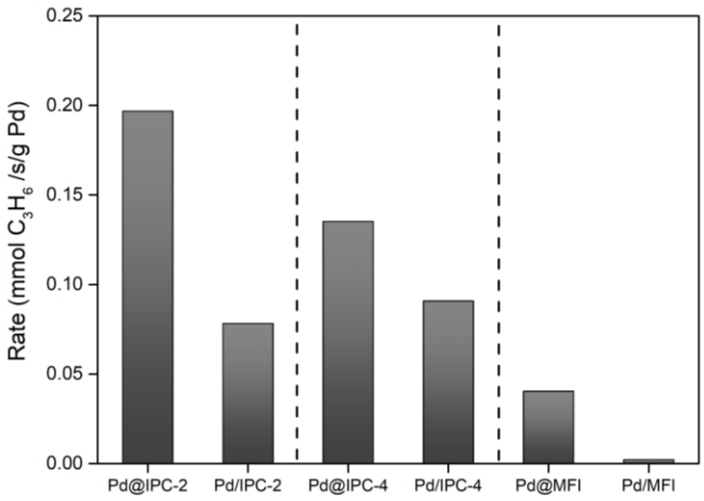

Figure 5. Rate of propene formation for encapsulated (Pd@IPC-2, Pd@IPC-4, Pd@MFI) and impregnated (Pd/IPC-2, Pd/IPC-4, Pd/MFI) catalysts in DH of propane, at 600 ˚C and TOS: 5 min.

The EDS measurements showed no change in the Pd content before and after the reaction for all the encapsulated and impregnated catalysts; therefore, the metal NPs were not leached out of the catalyst. However, it is known that the metal NPs tend to agglomerate and create larger particles, but in the

encapsulated catalysts, these particles are limited by the space inside the zeolite pores and channels, therefore their size is restricted even after the reaction, whereas the metal NP size of the impregnated catalysts increased significantly under the harsh condition of the reaction (**paper III, IV** and Figure 6). This presents another advantage of NP confinement, which prevents sintering and agglomeration of metal NPs and subsequently deactivation of the catalyst.

Regarding the higher rate of propene formation by Pd@IPC-2 compared to the other encapsulated catalysts (Figure 5), despite the fact that the intrinsic activity of Pd NPs in Pd@IPC-2 and Pd@IPC-4 for propane conversion are comparable (Figure 9) but the propene selectivity was higher for the Pd@IPC-2 catalyst (Figure 10) which resulted in higher rate of propene formation. The structure of the IPC-2 zeolite could explain a better chance for the mass transfer that lead to the higher productivity of Pd@IPC-2. This zeolite has larger pore system (12-ring: 5.6 x 7 Å and 10-ring: 6.1 x 4.7 Å) compared to the other studied zeolites in this study, that is IPC-4 (10-ring: 5.6 x 3.4 Å and 8-ring: 4.7 x 3.5 Å), and MFI (10-ring: 5.5 x 5.1 Å and 10-ring: 5.6 x 5.3 Å) [60]. Therefore, the produced gaseous molecules can escape outside the channels and pores more easily, and it might prevent generation of unwanted products via side reactions such as cracking. Moreover, for the least active encapsulated catalyst (Pd@MFI), there are acidic sites on MFI zeolite as an aluminosilicate structure that favor the side reactions and thus cracking was enhanced and subsequently selectivity to the desired product decreased significantly. It is noteworthy that in Pd encapsulated and impregnated within IPC-2 and IPC-4 supports, the metal NP sizes are similar, nevertheless the activity of metal particles in impregnated samples is significantly lower than the encapsulated ones, which means the activity of Pd NPs was improved in the confined space. In the case of Pd within MFI zeolite, the NP size in the impregnated catalyst is remarkably larger than the encapsulated sample, and due to the much lower specific surface area of the larger particles, there is an important impact on the drop in the activity. Therefore, it could be said that the intrinsic activity of Pd NPs is influenced by several parameters including the NP size, the interaction of the support with the NPs, and the diffusion limitation.

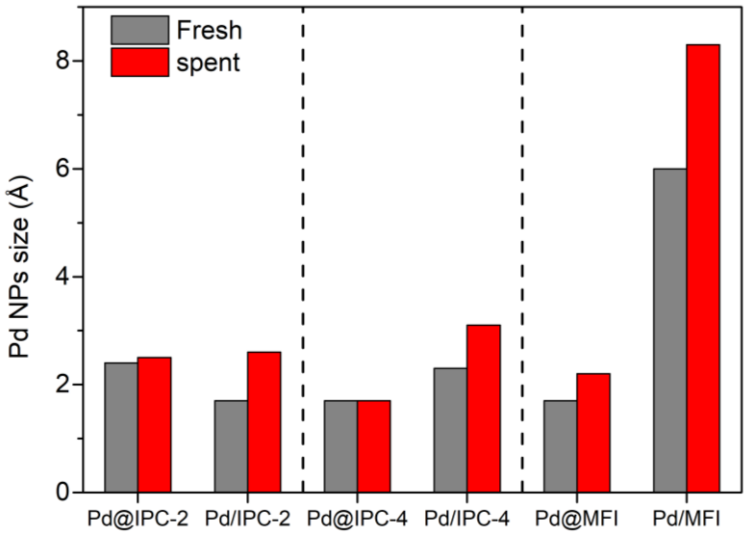

Figure 6. Pd NP size of encapsulated and impregnated catalysts before and after the reaction of propane dehydrogenation.

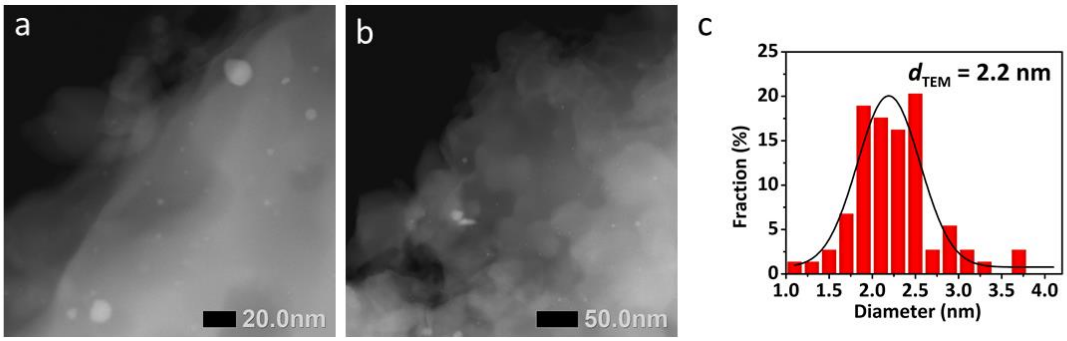

Figure 7. STEM images (a,b), and corresponding particle size histogram (c) of spent Pd@MFI.

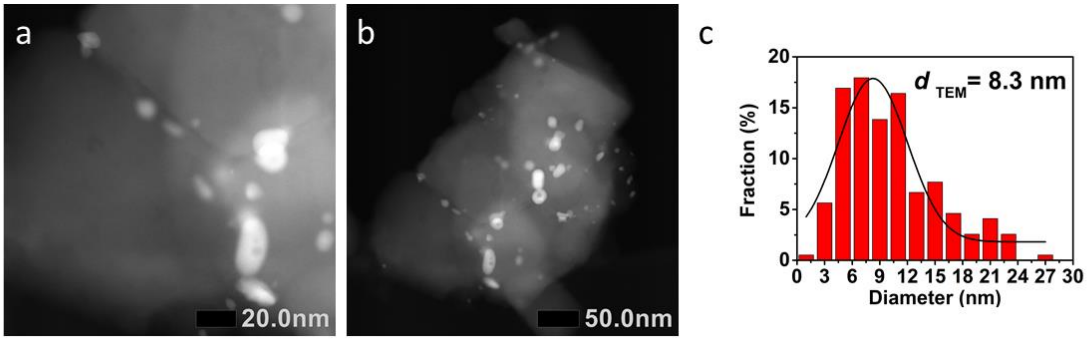

Figure 8. STEM images (a,b), and corresponding particle size histogram (c) of spent Pd/MFI.

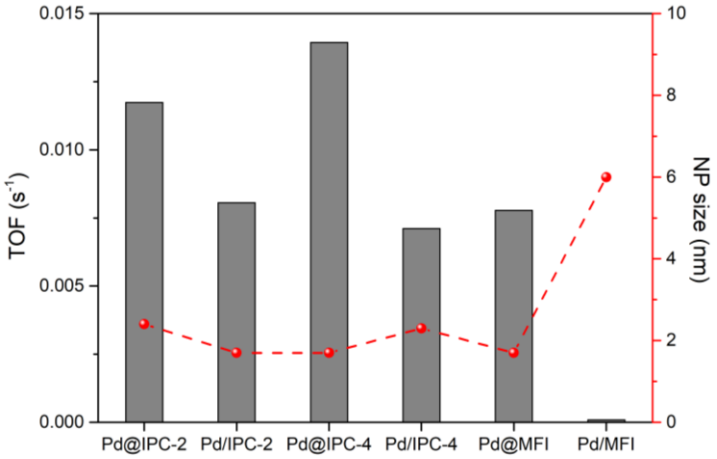

Figure 9. Turnover frequency of propane conversion on the surface atoms of the Pd NPs in encapsulated and impregnated catalysts with a comparison between Pd NP size in each catalyst, for TOS: 5 min

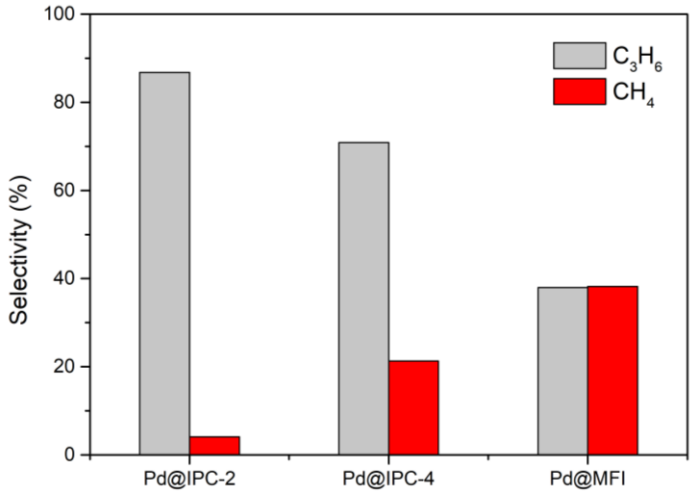

Figure 10. Selectivity toward propene and methane via different encapsulated catalysts, TOS: 5 min.

As expected, the catalysts exhibited a fast deactivation as it is typical for DH catalysts most likely as a result of the formation of carbon deposits at the active sites or in the pores. It could also be related to strongly adsorbed propene on the surface of the Pd NPs. Hence, cyclic catalytic tests become important for investigating the regeneration ability of these systems for long-term use. In the case of MFI zeolite, the encapsulated and impregnated catalysts are compared in Figure 11 and showed that both systems reach a plateau after 4 cycles, but in a way that the productivity and stability of the encapsulated samples are higher than those of the impregnated counterpart. In the encapsulated catalyst, the propane conversion exhibited a similar trend to the propene formation rate, shown in Figure 12. One of the possibilities is that the conversion decreased by enlarging the size of Pd NP during the cyclic tests and therefore blockage of the pores. Also, the dealumination of MFI zeolite during the reaction and regeneration steps could influence the activity by

decreasing the propane conversion. Since the acid sites are strong enough to favor the cracking reaction, dealumination and subsequent removal of the acid sites, resulted in an increase in selectivity towards propene and decrease in methane selectivity (Figure 12). On the other hand, for the impregnated catalyst, propane conversion increased during cycles while propene selectivity decreased (Figure 12). In the case of impregnated catalysts, probably the change in electronic structures of the metal particles on the outer surface of the zeolite assisted by the availability of the acid sites inside the empty pores led to an enhancement in propane conversion and methane selectivity. Nevertheless, eventually the activity (propane conversion and rate of propene formation) was limited maybe due to the dealumination that reduced the number of acid sites and also Pd NPs found an equilibrium size over time. Furthermore, it was observed that, in fact, the cracking, which is a side reaction, was improved, not the propene selectivity (Figure 12). Therefore, in the end, the rate of propene formation for the impregnated catalyst was leveled off under the value for the encapsulated catalyst (Figure 11). Note that the selectivity of propene and methane cannot be compensated by each other, and as the selectivity to ethene was not in line with methane, thus it means when cracking was favored and selectivity towards methane increased, some other carbon side product (which could not be detected by the used GC column) by means of different mechanisms were generated.

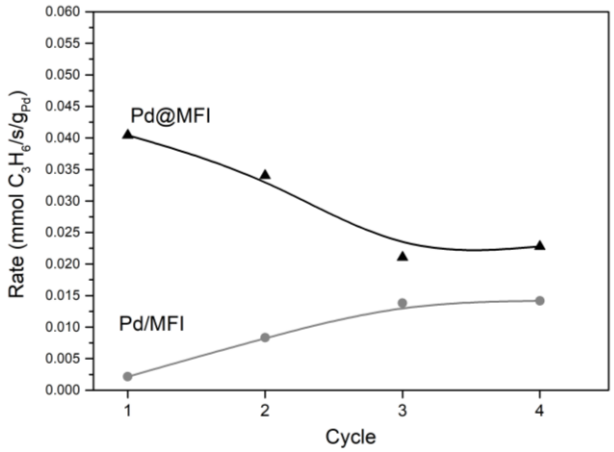

Figure 11. Rate of propene formation for the dehydrogenation catalytic cyclic test of encapsulated (Pd@MFI) and impregnated (Pd/MFI) at TOS: 5 min.

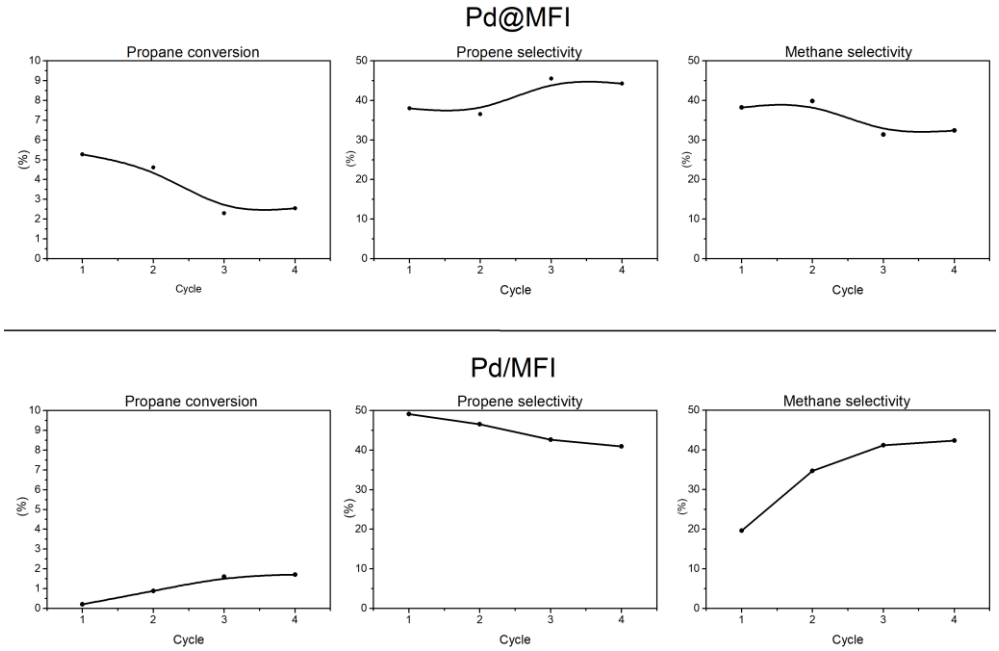

Figure 12. Propane conversion, propene and methane selectivity over the cyclic catalytic test for Pd@MFI and Pd/MFI, TOS: 5 min

Regarding the IPC-2 and IPC-4 zeolites, different behavior was observed. Similarly, the encapsulated catalysts exhibited higher activity in the first cycle, but then dropped sharply after the regeneration, while the impregnated samples exhibited lower activity, but almost without a big change (Figure 13). The XRD patterns revealed that although the transformation from UTL zeolite to IPC-1P and then IPC-2 and IPC-4 took place without any problems and the structure has been preserved after the introduction of the metal NPs (**Paper IV**), the structure of the encapsulated catalysts collapsed under the harsh reaction and regeneration conditions, and at the same time under the stress associated with the presence of Pd NPs between the individual lamellae, as the main peaks at 7.6 ° and 9.7 ° 2θ disappeared in the XRD patterns of the spent Pd@IPC-2 and Pd@IPC-4 catalysts, respectively (Figure 14). Thus, structural collapse was the reason for the decreased activity of the encapsulated catalysts after the first cycle of dehydrogenation. Note that Pd in impregnated samples did not cause stress and tensions and the zeolite structure was much more stable. Also, for the MFI catalysts, both encapsulated and impregnated samples exhibited stable structure after the reaction and regeneration step (Figure 15). The higher stability of MFI is caused by the thicker layer of this zeolite compared to the other two, as one unit cell layer is thicker than layer in UTL-derived zeolites, and in addition, MFI sample consists of “layers” containing more than one unit cell, thus the structure is more rigid. Furthermore, there was no peak showing the presence of crystalline Pd in any of the studied catalysts in this work.

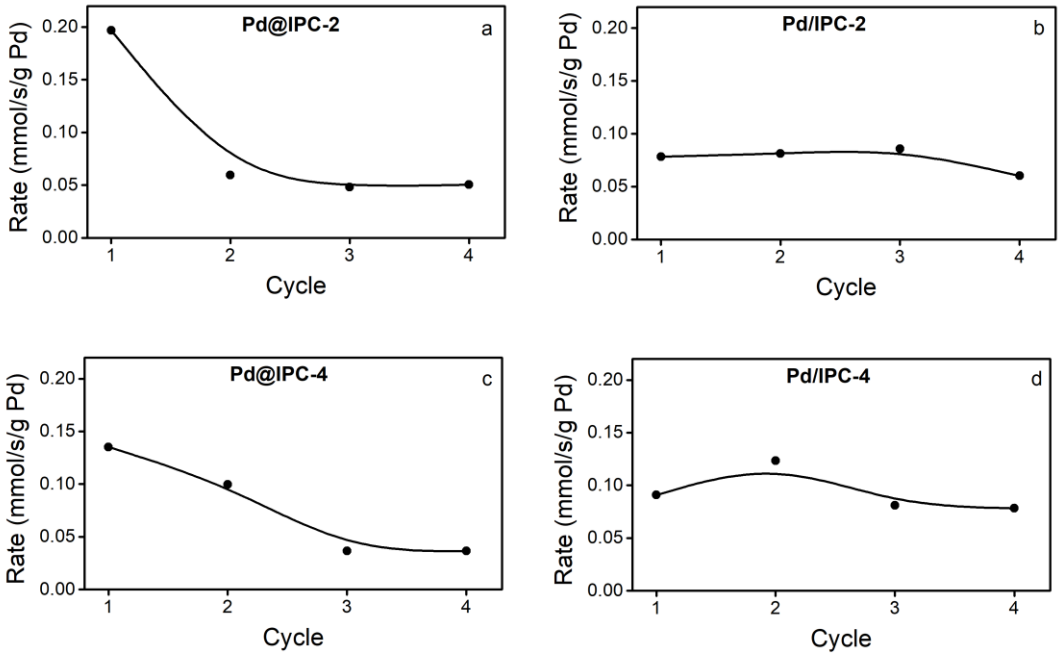

Figure 13. Initial activity of the Pd@IPC-2 (a), Pd/IPC-2 (b), Pd@IPC-4 (c) and Pd/IPC-4 catalysts expressed as the rate of propene production for four cycles.

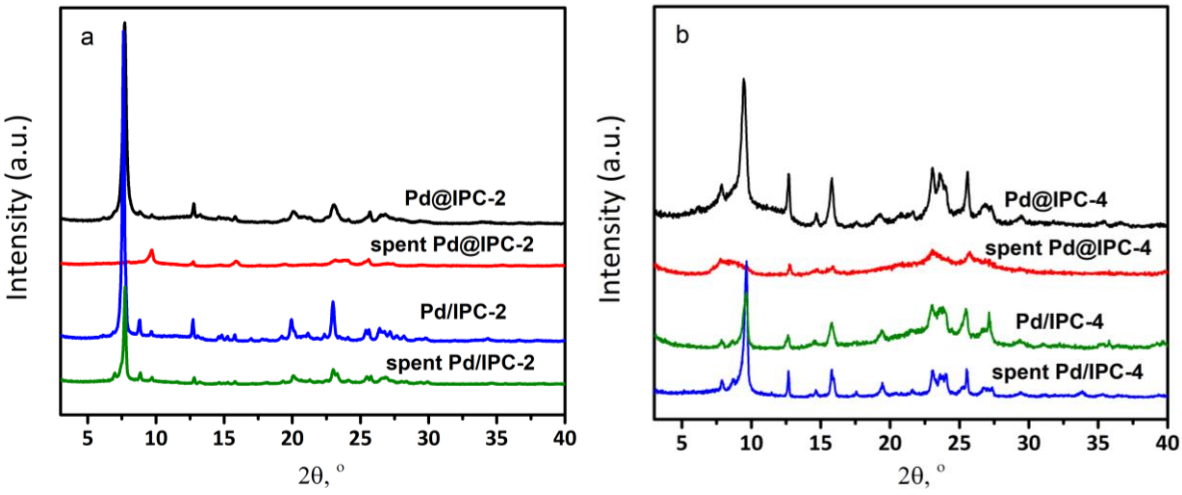

Figure 14. XRD patterns of fresh and spent encapsulated and impregnated Pd-IPC-2 (a), and Pd-IPC-4 (b)

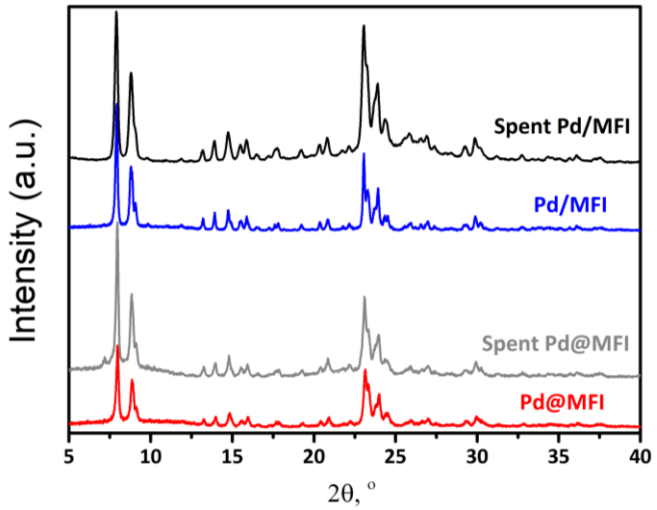

Figure 15. XRD patterns of fresh and spent encapsulated and impregnated supported Pd NPs within MFI zeolite.

The textural properties of the studied catalysts were evaluated using N_2 adsorption-desorption isotherms (**Paper III and IV**), demonstrating type I for microporous materials according to the IUPAC classification [61] and confirmed the reduction of the BET (Brunauer-Emmett-Teller) surface area and micropore volume of the catalysts compared to the parent zeolite. These smaller values are due to the partially occupied pore by the metal NPs. After the reaction, the BET surface area and micropore volume of the spent catalyst (without regeneration) was measured and showed even lower values, but this time as a result of carbon deposit formation during the dehydrogenation reaction which could be the reason for the fast deactivation of the catalyst under the reaction stream (**Papers III and IV** and Figure 16).

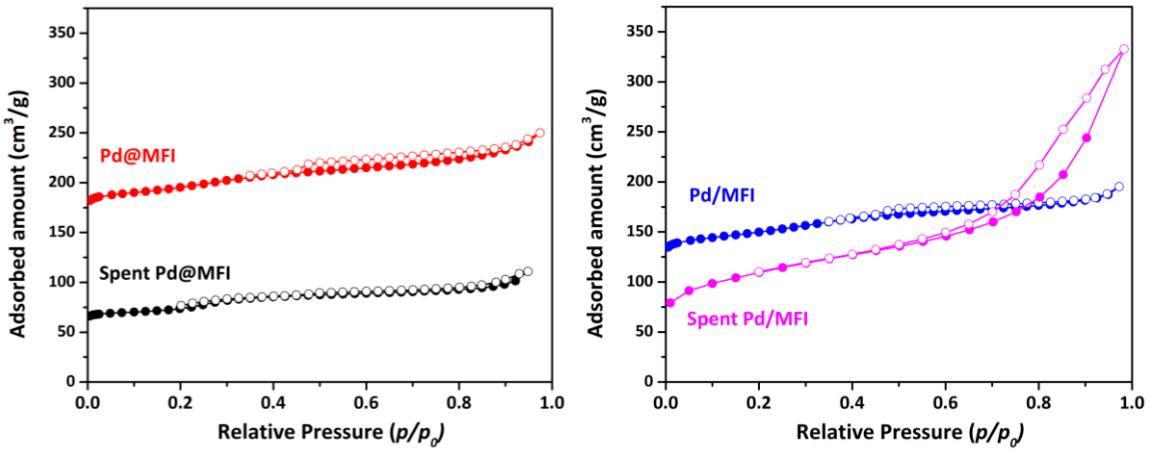

Figure 16. N_2 physisorption isotherms of the fresh and spent encapsulated (left) and impregnated (right) supported Pd within MFI.

As Pd@IPC-2 and Pd@ IPC-4 exhibited higher productivity for the dehydrogenation reaction, more research was performed to study their behavior. For example, different amounts of carbon deposit were

detected by the TG-DSC shown in **Paper IV**. It was discussed that the confinement of the Pd NPs resulted in a lower content of carbon deposit. Also, the diffuse-reflectance FTIR (DRIFT) technique was used to monitor the availability of the active sites by the CO probe molecule. It was observed that there are two absorption bands of carbonyl formed on metallic Pd, linear and bridged carbonyl. The integral intensities of the linear and bridged carbonyls revealed that in the impregnated catalysts the intensity of the linear carbonyls decreased after the reaction, whereas it increased for the bridged carbonyls during the reaction, because Pd NPs tend to form larger particles from unprotected Pd atoms after the reaction on impregnated catalysts, in line with the STEM results of the NPs size evaluation. In the case of the encapsulated catalysts, the intensity of both linear and bridged carbonyls decreased as the active sites are less accessible because the zeolite framework collapsed, as evidenced by changes in XRD and textural properties of spent materials (decrease in the volume of micropores accompanied by increase in external surface area, see **paper IV** Fig. 9) and therefore the probe molecule as well as the reaction feed could not reach the metal NPs.

Based on this section, it could be concluded that in the catalytic activity of Pd NPs encapsulated within MFI, IPC-2 and IPC-4 zeolites in the direct dehydrogenation of propane, there are a couple of effective factors that influence catalyst activity, including the size of the nanoparticles and zeolite channels, electronic structure of the metal NPs, and structure of the support framework. Overall, the encapsulated Pd NPs show a higher propane conversion and propene formation rate compared with their impregnated counterparts, probably because of the smaller size or intrinsic properties of confined Pd NPs. The confinement of Pd NPs within a zeolite framework prevents undesired sintering, whereas their size increases in the impregnated catalysts during the reaction. Furthermore, even though the Pd NPs encapsulated within the IPC-2 and IPC-4 catalysts show a decrease in coke deposition inside the pores, their structures collapsed, meaning that the Pd active sites were inaccessible after the reaction and consequently caused deactivation during cyclic catalytic tests.

4.3. Boron nitride

In this part of the thesis, commercial hexagonal boron nitride was studied as a catalyst for oxidative dehydrogenation of propane due to its high activity and selectivity while preventing overoxidation [45, 48]. The goal was to better understand catalytic behavior of this system as it was reported a high promising catalyst with many unclear aspects. Thus, the catalyst activity was measured under various conditions such as different atmospheres, time on stream, temperatures, catalyst masses, reactor diameters, etc. The fresh and spent catalysts were characterized with a wide range of methods to investigate the physicochemical changes occurring on the catalyst during the reaction, and also to find out the actual role of the catalyst in this system. Our findings were confronted with the views on the reaction mechanism and the role of the hBN catalyst published in the literature. Although it has been firstly hypothesized in the literature that the

boron oxide acts as the active site, and also gas-phase reactions are involved [51, 52], but the knowledge about how active sites function and the mechanisms need to be unveiled. Grant et al. first suggested that >B-O-O-N< was the active site [45] which was invalidated by observation of the oxidized boron structure generated on boron containing materials with similar ODHP activity [47]. Both theoretical and experimental studies on the catalytic activity of hBN catalytic systems identified the oxygenated boron species as active sites [46, 62]. The generation of the oxygenated boron species in this catalytic system is studied and discussed in **Paper I.** It was shown that the oxyfunctionalization of hBN is not limited only to the surface of the catalyst but also a deep penetration into the volume of the particles was observed. Su et al. found that the hBN materials could not be oxidized below 800 °C under an O_2 atmosphere, indicating that with molecular O_2 alone it was difficult to form the proposed B−O species at the armchair edges under ODH reaction conditions [63]. Therefore, as a part of our study, different atmospheres were applied at the reaction temperature (490 ˚C) to study the possible physicochemical changes in an inert, oxidative, propane and ODHP environment. The results revealed that only the ODHP reaction atmosphere ($He/O_2/C_3H_8$), which contains propane and oxygen simultaneously, make changes in the chemical composition, crystallinity, and surface area of hBN in agreement with Su's group [63]. Figure 17 shows the changes in chemical composition of hBN treated in different atmospheres. It was observed that neither propane nor oxygen could change the catalyst chemical composition independently, where hBN showed stability on the surface and inside the bulk. The N_2 adsorption-desorption isotherms of the fresh and treated samples, shown in Figure 18, exhibit character similar to type II based on IUPAC classification for non-porous or macro-porous materials [61] and also did not go through significant changes in different single atmospheres. But, when propane and oxygen were fed simultaneously to the reactor, an obvious increase in oxygen content occurs accompanied by a decrease in nitrogen content (Figure 17). The oxygen content on the catalyst surface changes significantly from 5 to 13 at. % for the fresh and activated samples, respectively, confirmed by XPS, while the EDS results showed that it changed slightly from ca. 2 to 5 at. % inside the bulk. Also, the BET surface area declined from 46 to 25 $m^2 g^{-1}$. Therefore, it displays that the interaction between reaction precursors and the catalyst, stimulate the catalyst to generate oxygenated species. These changes are more noticeable on the surface of the catalyst based on the XPS data, because the surface is more exposed and is readily available for the feed molecules. As the melting point of the boron oxide is lower than the ODHP reaction temperature, the accessibility of gaseous probe molecule (nitrogen) to the catalyst surface had been reduced on partially fused surface and caused the decrease in BET surface area. Furthermore, the amount of nitrogen declined on the surface from 46 to 40 at. % (XPS) and inside the bulk from 50 to 47 at. % (EDS), whereas boron content was kept almost constant, 47 at. % on the surface and 50 at. % inside bulk. The XRD patterns of the fresh and the treated catalysts (Figure 18) confirmed the formation of crystalline BO_3 only under a reaction atmosphere that agrees with the XPS and EDS results. The diffraction peaks at 14.6 ˚ and

27.9˚ 2θ correspond to BO_3 (Crystallography Open Database (COD) code: 2016172), while the peaks at 26.7˚, 41.7˚, 43.8˚ and 55˚ 2θ are related to the hexagonal structure of hBN (COD database code: 9008997). Furthermore, Raman spectra of the treated hBN shown in Figure 19 confirmed the generation of B-O and B-O-B bonds, peaks at 882 and 500 cm^{-1} Raman shifts, respectively. Their presence is visible only when the treating atmosphere contains propane and oxygen concurrently. The peak at 1367 cm^{-1} that is related to B-N is clearly observable in all spectra.

Our observation confirms part of Su et al. hypothesis [63], where hBN materials found being not able to be oxidized under an O_2 atmosphere (below 800 °C), indicating that molecular O_2 alone is not able to attack surface of hBN and to form the proposed B−O species at the armchair edges under ODH reaction conditions. Our results show that the oxidation occurs under the ODHP reaction atmosphere and temperature (490 °C) not only at edges, but also gradually inside the bulk hBN (**Paper I**).

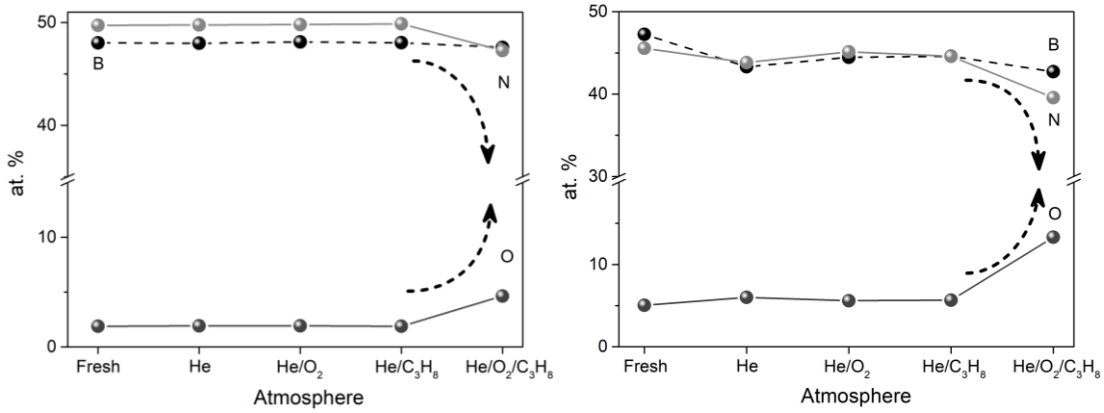

Figure 17. Chemical composition of hBN treated under different atmospheres analyzed by EDS (left) and XPS (right).

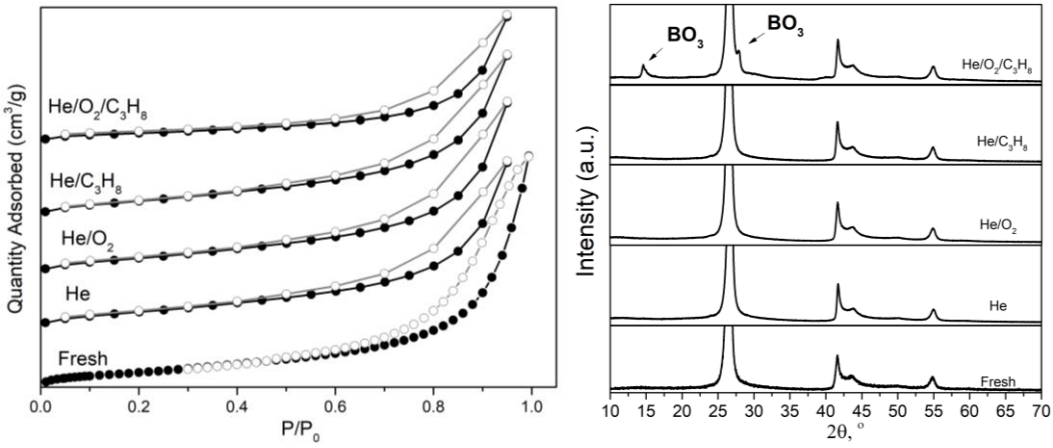

Figure 18. N_2 adsorption-desorption isotherms (left) and X-ray diffraction patterns of the treated hBN under different atmosphere.

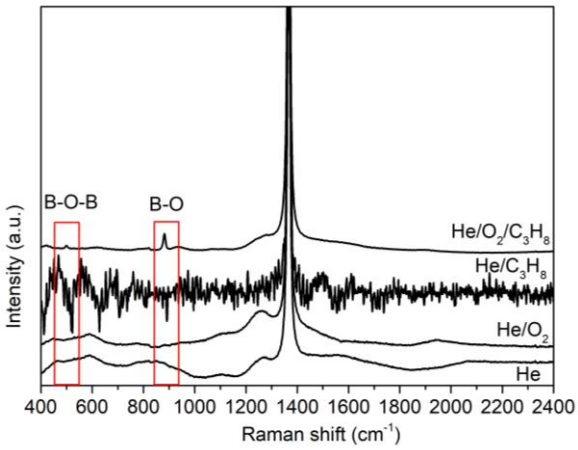

Figure 19. Raman spectra of the treated hBN under different atmospheres.

In some of the first studies, an amorphous boron species like oxyhydroxide ($B(OH)_xO_{3-x}$) layer was identified on the surface of hBN as the active sites [48, 64]. On the other hand Shi et al. proposed that it is the hydroxylated B-OH that acts as the active site [46, 62]. Later it was concluded that the hydroxylated boroxol ring/tri-coordinated planar oxidized boron is the active site and B-OH reacts with O_2 to produce >B-O-O-B< sites that can abstract hydrogen from propane [62, 63]. Shi et al. further studied the participation of BO_x active species in ODHP reaction by using in situ FTIR characterization and isotopic labeling experiments. In situ IR spectroscopy demonstrated that the intensity of B−OH vibration which was claimed to be around 3400 cm^{-1}, continually weakened with the introduction of O_2 to the propane atmosphere. This phenomenon demonstrated that B−OH was an active surface intermediate involved in the reaction network. Isotope labeling experiments discovered that both HDO and D_2O were generated when C_3H_8 and O_2 were introduced into the deuterated BNOD catalyst at 530 °C. The $H_2{}^{16}O$ and $H_2{}^{18}O$ signals also appeared after the catalyst was exposed to $^{18}O_2$, indicating that two adjacent B−OH were able to dehydrate and reversibly exchange H and O atoms with gas-phase reactants. A Langmuir-type dependence on oxygen concentration (0.5) and second-order dependence on propane concentration demonstrated that the molecular oxygen was adsorbed or activated on the catalyst surface and that the propane derived from the gas phase directly reacted with the active oxygen species [46].

In our research the functionalities and the skeletal vibration of the hBN catalyst before and after reaction was identified by DRIFT spectroscopy. To make the comparison more visible, the spectra from the spent catalysts are subtracted from the spectra of the fresh hBN and shown in Figure 20. The intensity of the peaks at 732 cm^{-1} and 1200-1300 cm^{-1}, corresponding to B-O vibration, increases by reaction time, which confirms the generation of B-O bond, in agreement with the EDS and XPS results (Figure 21) showing the increment in oxygen content of the catalyst. Also, the XRD patterns (Figure 22) exhibited formation of boron oxide crystalline phase during TOS which is accompanying by increase in boron oxide crystallite size while boron

nitride crystallite size is almost constant (Figure 22). On the other hand, our observation not fully agrees with Shi et al. report discussed above [46]. There are two points where there are disagreement, first the vibration at 3400 cm^{-1} is probably corresponding to N-H [63, 65] and also its intensity is constant over time (Figure 20). Moreover, the O-H vibration is more likely to appear in higher frequency [65], therefore in this research the O-H vibration is considered at 3690 cm^{-1} (Figure 20). Furthermore, the O-H vibration at 3690 cm^{-1} was interrupted in the initial step under the stream and its intensity decreased from the beginning and not gradually, which could be due to formation of the real active sites at the very first stages of the reaction. Hence one scenario could be that the O-H vibration was interrupted because of the interaction with reaction feed or radicals produced in the feed, and thus the O-H group on the surface of the hBN is involved in the reaction. This agrees with the previous researches that announced the participation of oxygen from the edge hydroxylated boron nitride [46, 62, 63], however not a step by step decrease at 3400 cm^{-1}, but an instant decline at 3690 cm^{-1}.

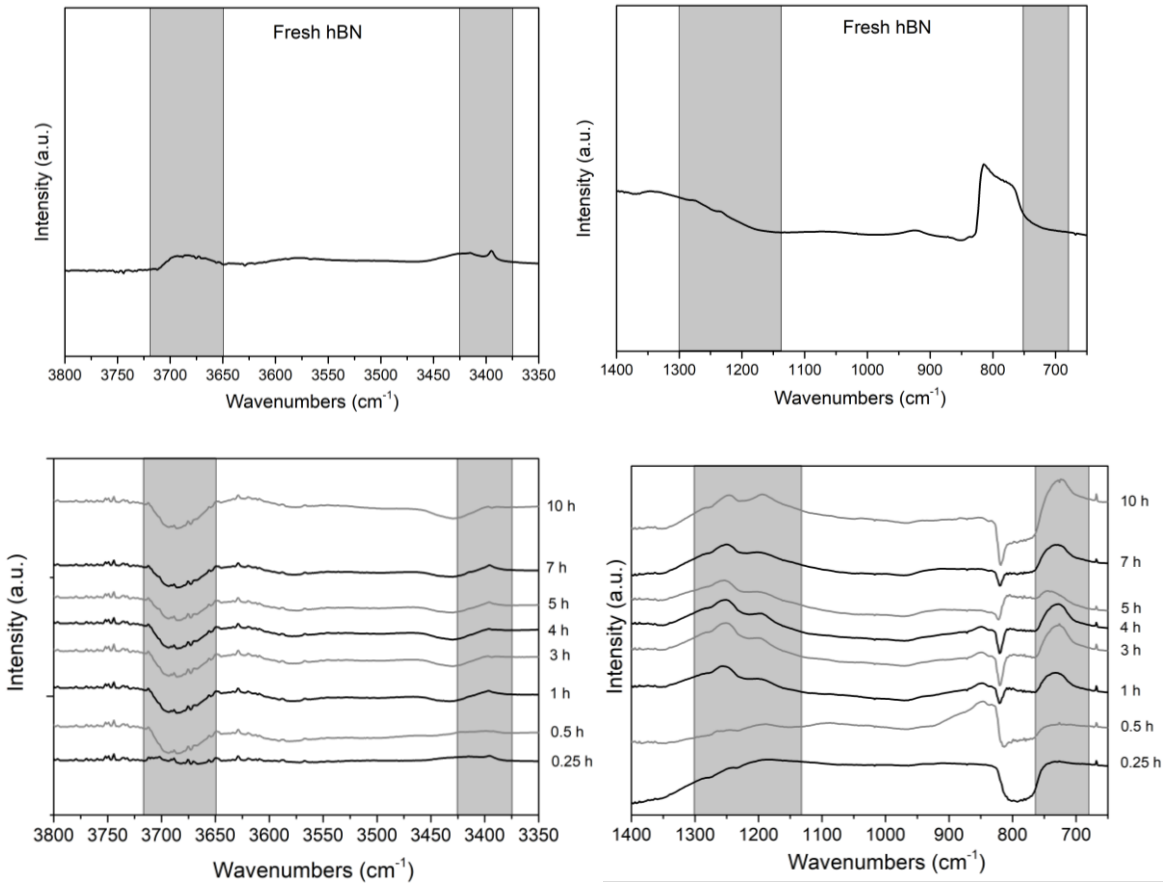

Figure 20. DRIFT spectrum of fresh hBN in the range 650-1400 cm^{-1} (above right) and and 3350-3800 cm^{-1} (above left). The subtraction of DRIFT spectra collected through spent hBN from the fresh hBN for the corresponding ranges (below).

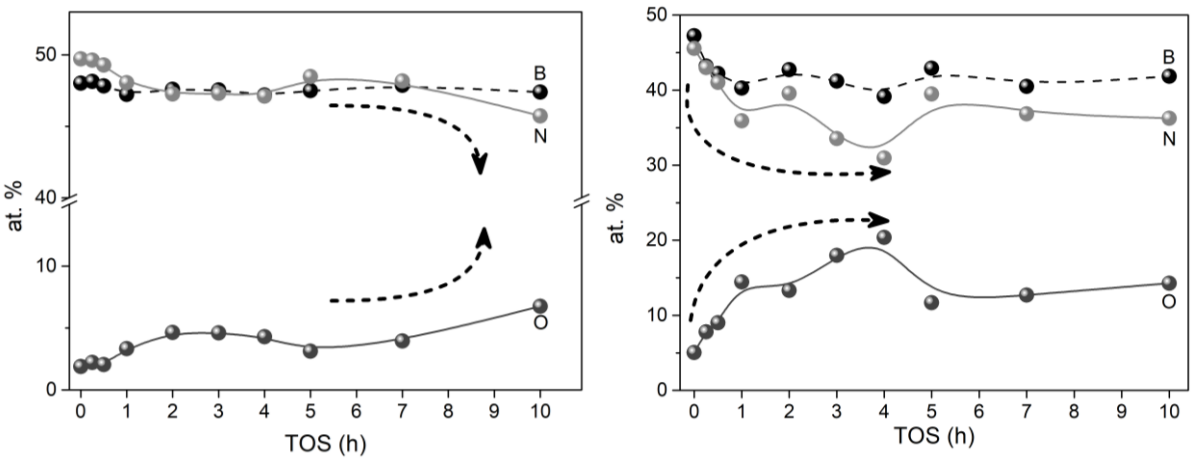

Figure 21. Chemical composition of hBN under the ODHP reaction atmosphere as a function of time on stream analyzed by EDS (left) and XPS (right).

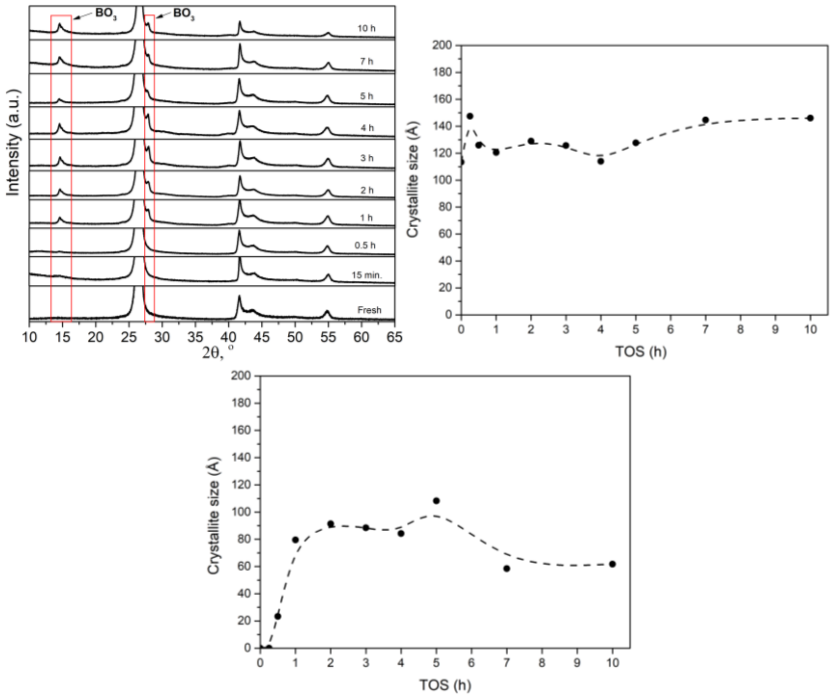

Figure 22. X-ray diffraction patterns of the treated hBN under different time on stream (left), crystallite size of hBN (middle) and BO_3 (right), calculated by Scherrer equation for 2θ: 26.5 and 14.5, respectively.

Later it was reported that propene is mainly generated on the catalyst surface (BO_3 site) while C_2 and C_1 products are formed via both surface-mediated and gas-phase pathways. This was the first direct experimental evidence of gas-phase methyl radicals ($CH_3^{\bullet}$) in the ODHP reaction over boron-based catalysts that was achieved by using online synchrotron vacuum ultraviolet photoionization mass spectroscopy (SVUV-PIMS), and uncovers the existence of gas-phase radical pathways [52], Meanwhile, any gas-phase ethyl ($C_2H_5^{\bullet}$) and propyl ($C_3H_7^{\bullet}$) radicals were not detected in this system, meaning the main product

propene, is more likely formed on the catalyst surface, since no gas-phase propyl radicals were observed. [50, 52]. Recently, it was discussed that to initiate the radical chain reactions in the gas phase, O_2 is activated on the boron site to form BOO$^{\bullet}$ which react with propane to generate $C_3H_7^{\bullet}$ and HOO$^{\bullet}$ radicals. Later the former one oxidized by O_2 and the later one act as H-abstractor to react with another propane [66].

After these reports, instant screening of the catalyst behavior and generated products became crucial. Accordingly, the experiments were performed in the presence or absence of O_2 and reaction mixture (RM) by means of mass spectroscopy. The hBN samples (and SiC as a blank test) were treated under the ODHP atmosphere for various time periods in the stream and then the oxygen or reaction mixture was terminated while the changes in products were continuously monitored. The mass spectra disclosed that after termination of the dosing reaction mixture or oxygen over hBN, water formation did not end immediately but decreased gradually over time, unlike in SiC, where water peak intensity dropped immediately (Figure 23). Moreover, the desorption of water from the samples that were treated for longer time, occurred with prolonged delays compared to the ones treated in shorter time. For example, it is clearly visible that water was more easily desorbed from the hBN surface that was treated for 25 minutes rather than 3.5 hours (Figure 23). Therefore, it could be understood that water was formed on the surface of hBN catalyst and that this is the reason why after termination of the reaction mixture or oxygen, water was still detected and was kept desorbing over time. There are a couple of explanations for such different desorption kinetics of each sample, for instance, it could be the fact that a different amount of water was formed on the surface depending on time under the ODHP stream. It also might be related to the different types of adsorption sites which were generated during time; thus, desorption took place with different mechanisms. Moreover, it can be said that due to diffusion limitation, a different time was needed for desorption. It also could be caused by dehydroxylation of the surface at 490 ˚C, where the OH groups generated during the reaction on the surface are unstable in inert gas stream. On the other hand, when the dosing of the reaction mixture or oxygen was interrupted, the oxygen decreased immediately and dramatically (Figure 23). This means that there was no oxygen adsorbed on the surface of hBN as a molecule that would desorb over time and gradually decrease the detection of oxygen. Therefore the detected oxygen was probably only from the gas phase, while the adsorbed oxygen (which increased the oxygen content of the catalyst after the reaction) probably was dissociatively chemisorbed, in agreement with DFT calculation showing irreversible oxygen functionalization of the fresh edges [67]. Regarding the formation of the products, propene as the main product, ethene as the main side product and methane as the cracking product were also ended rapidly by termination of reaction mixture (Figure 24). But after discontinuing dosing oxygen, these products were still detected for longer time, gradually decreasing before reaching the initial states. Thus, the results revealed that the reaction products are either formed on the surface of the catalyst or they are adsorbed on the surface after being generated in the gas phase and then escaped in the absence of oxygen by the stream, over a short

period of time but not instantly. Furthermore, the combination of these results (showing no detection of O_2 molecule by MS and no change in O content by treatment of hBN only under oxidative atmosphere) disagree with the reports considering the adsorption of the O_2 molecule on the hBN surface as a molecule to generate oxygenated boron species. A complementary experiment of dosing oxygen for a certain short period of time (oxygen pulse dosing while propane was flowing) revealed more important information. The results have shown that when propane and oxygen co-exist in the reaction feed, immediately propane conversion was initiated and reached 17% propane conversion, (Figure 25) which means the reaction starts instantly and independently from the formation of oxygenated boron species over time. This result is against some reports mentioning the idea of necessary induction period for formation of boron oxide as the active site, because in this pulse experiment with short time of dosing oxygen, no induction period was required. Also, in our catalytic measurements any induction period was never observed. Therefore, all together could support the hypothesis that the ODHP reaction starts via formation of radicals in the gas-phase and stand against the frequent report of introducing boron oxide as the main driver in this system. In other words, the gas-phase reaction is the reason for the oxyfunctionalization of a hBN surface and not the consequence of that phenomenon. The reason is probably that the radicals formed in the gas phase activate the hBN surface and result in an increase in the oxygen content on the catalyst surface. This experiment was performed three times, and each time the results were repeated without showing any history effect, revealing that the formation of oxygenated species on the hBN surface does not influence the main driver of the reaction which is the gas phase. It could also be said that at the beginning of the reaction, the catalyst surface might be the location for termination of the generated radicals in the gas phase.

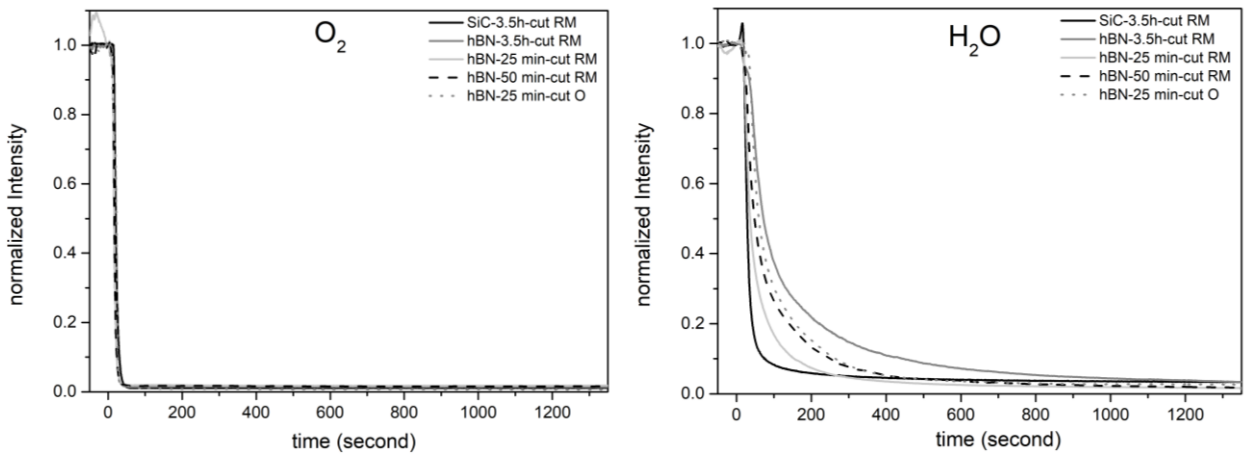

Figure 23. Detection of oxygen (left) and water (right) during ODHP as a function of measurements time in mass spectroscopy after termination of RM and O_2.

Reactor id: 15.5 mm, T: 490 ˚C, mass of catalysts: 100 mg, $He/O_2/C_3H_8$ = 11/3/6 ml min^{-1}

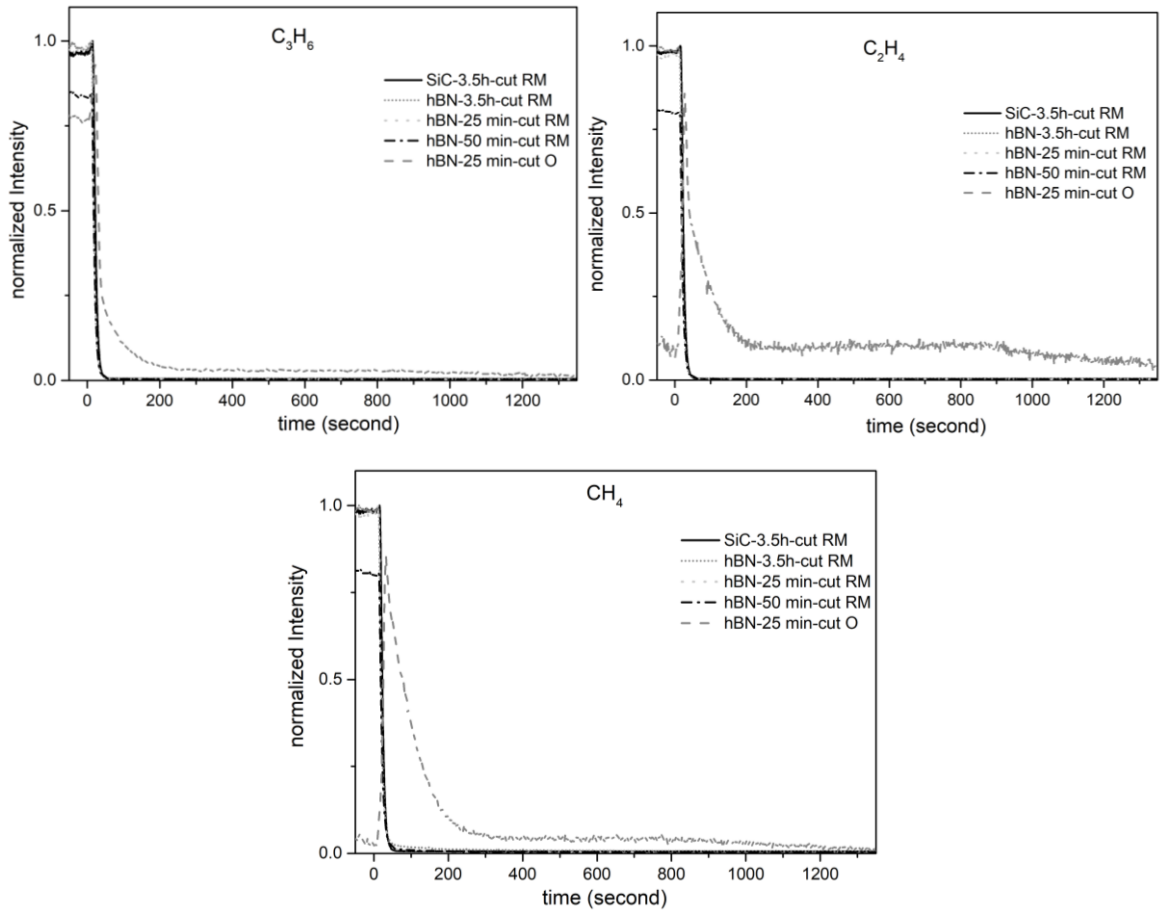

Figure 24. Propene, ethene, and methane mass spectra during ODHP as a function of measurements time in mass spectroscopy after termination of RM and O_2. Reactor id: 15.5 mm, T: 490 ˚C, mass of catalysts: 100 mg, $He/O_2/C_3H_8$ = 11/3/6 ml min^{-1}

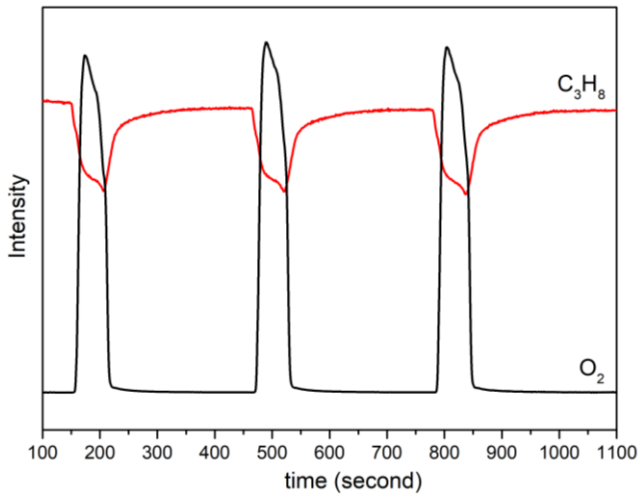

Figure 25. Mass spectra of oxygen and propane when oxygen was dosed as a pulse experiment. Reactor id: 15.5 mm, T: 490 ˚C, mass of catalysts: 100 mg, He/C_3H_8 = 11/6 ml min^{-1}, O_2: 3 ml min^{-1}

Although several studies have indicated that the ODHP reaction is driven by a combination of surface and gas-phase reactions over boron-based catalysts [48, 51, 53, 54] the exact contribution from each side and the mechanism has not understood yet. The important parameter that has been frequently overlooked is the size and geometry of the reactor and arrangement of the catalytic bed. In fact, this parameter is a representative of available free space for the gas-phase reaction. There are few reports focused on this topic where it was tried to study the effect of free space on hBN activity [54, 66, 68] and they will be compared to our results in the following parts.

In our first step, to understand the influence of reactor and catalytic bed geometry on gas-phase chemistry of reaction, the ODHP reaction over hBN was studied by utilizing different size of reactor and realization of catalyst bed to provide various free space (**Paper V**). Interestingly, the propane conversion increases with changes in product selectivity as a function of reactor free space (Scheme 2, and Figure 26), which agrees with Venegas work reporting decrease in propane conversion by changing the reactor diameter from 8 to 4 mm [54]. To take a step forward, two reactors with the same free volume but different diameter of the catalyst bed (Scheme 2, reactor 5 and 6) were used to test the effect of reactor geometry at constant free volume on course of the ODHP reaction. These two reactors exhibited similar activity regardless of the differences in diameter, therefore it could be said that the gas-solid interface does not play a key role, but in fact the available free space drives the conversion of propane. This phenomenon is connected to the fact that the change in the reactor geometry not only impact the free volume, but also influence the residence time of the reaction mixture within the available space (**Paper V**). Note that although the interaction period with catalysts (contact time) remains the same, the residence time within the space is affected. Therefore, it confirms the vital role of gas-phase reactions and to support this idea, more experiments were carried out. The reactor was also fed by reverse direction (Scheme 2) to check the effect of post-treated free space in the gas-phase reactions, and it confirmed the preliminary observations (Figure 26) but the propane conversion decreased over time which was not observed for direct feeding with free space above the hBN catalyst (Figure 27). The chemical composition analysis of the spent catalysts after 3 hours of reaction by EDS revealed that in both feeding pathways, the oxygen content (which represents the oxygenated boron species) increases as the free space inside the reactor expands (Table 4). In the direct feeding, the lowest amount of oxygen (3.2 at. %) was observed for the smallest reactor with 9 mm diameter, while this value increased step by step for each reactor by enlarging the container and reached 15.6 at. % for the largest reactor with 15.5 mm diameter. The amount of boron was almost constant, while the nitrogen content slowly decreased, probably due to the substitution with oxygen. In general, this trend was also valid for the reverse feeding direction, but with a lower oxygen content that changed from 2.6 to 7 at. % for the smallest and largest reactors, respectively. It seems that the amount of incorporated oxygen is proportional to the amount of converted propane because the lower activity of hBN under the stream due to the deactivation (Figure 27)

is corresponding for the lower content of oxygen in the reverse direction of feeding. Concerning this observation, it also could be deduced that the position of the catalyst bed could influence the activity, and the free space above the catalyst surface provide a better environment for the radicals to attack the catalyst surface and form the products, or maybe generates species that participate in the reaction and enhance the activity. Due to the interaction of feed molecules with each other in the gas phase that results in generation of radicals (probably oxygenated propyl radicals) the hBN surface is activated, but in the reverse feeding with post-treatment free space, the residence time assist only in the formation and propagation of the radicals that not all of them will meet the catalyst surface eventually. Therefore, it was observed that the availability and the position of the free space is evidently crucial and have impact on oxygen content of the catalyst which is a representative of how much gas-surface interaction was involved (**Paper V**).

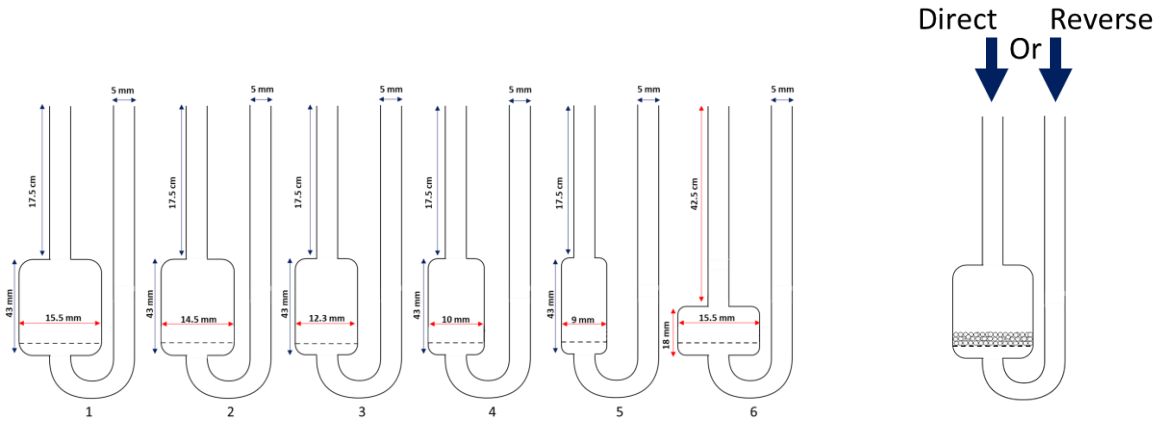

Scheme 2. Schematic of the prepared reactors for ODHP over hBN (left) and the applied direct and reverse feeding lanes (right).

The free volume above the catalyst bed: Reactor number 1: 5.4 ml, 2: 4.9 ml, 3: 3.4 ml, 4: 2 ml, 5: 1.4 ml, 6: 1.4 ml.

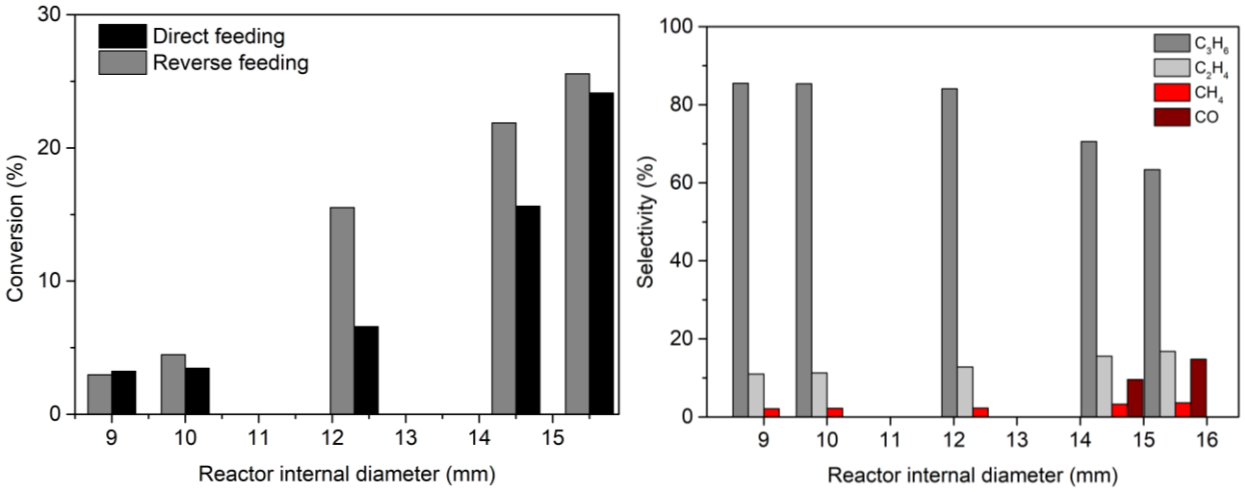

Figure 26. Propane conversion as a function of reactor size in ODHP for direct and reverse feeding direction (left), and products selectivity for the direct feeding (right), T: 490 ˚C, mass of catalysts: 100 mg, TOS: 15 min., $He/O_2/C_3H_8$ = 11/3/6 ml min^{-1}

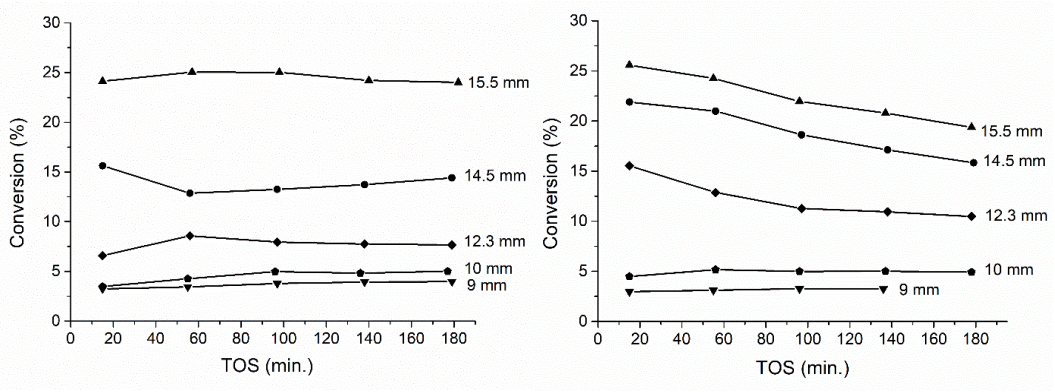

Figure 27. Propane conversion as a function of TOS for different reactor sizes under the ODHP atmosphere, the direct direction of feeding (left), and the reverse direction of feeding (right). T: 490 ˚C, mass of catalysts: 100 mg, $He/O_2/C_3H_8$ = 11/3/6 ml min^{-1}

Table 4. Chemical composition of spent hBN after the ODHP reaction via different reactor sizes (Figure 27), TOS: 180 min.

		at. %		
	Reactor diameter (mm)	B	N	O
Direct	15.5	45.1	38.5	15.6
	14.5	47.2	46.0	5.9
	12.3	47.5	47.1	4.5
	10	47.5	47.7	3.7
	9	47.7	48.2	3.2
Reverse	15.5	47.1	45.1	7.0
	14.5	47.3	46.5	5.3
	12.3	47.4	47.2	4.4
	10	47.4	48.7	2.9
	9	47.9	48.9	2.6

Lindstedt et al. further stated that the catalyst is only responsible for initiating the gas-phase chemistry and the gas-phase is responsible for the high selectivity toward olefins [51]. Different radicals desorbed from the surface of catalyst can initiate the gas-phase reactions and influence the product distribution [48, 51, 53, 54, 69]. According to the numerous research that have shown partial oxidization of hBN, it has been frequently reported that the initiation of radicals occurs on the surface of hBN and multiple boron oxide species are proposed as the active sites [64, 67, 70, 71]. Boron peroxyl radical (BOO•) formed by reaction between O_2 and tri-coordinated boron, is proposed to serve as the initiator of the gas phase radical chain by reacting with propane to form C_3H_7• and HOO• radicals [71]. In agreement with the hypothesis that states oxidized boron species as the active sites [45, 53, 72, 73], it was reported that either the B_2O_3 has identical catalytic property regardless of supports or the product distribution is determined in the gas phase reaction rather than the B_2O_3 surface [66]. As the boron oxide melting point is lower than the ODHP reaction temperature, it was reported that the presence of dimerized di-coordinated boron radical >B-B< dynamically formed in the liquid boron oxide activates O_2 molecule to form peroxide-like >B-O-O-B< sites. Then propane is oxidized on those sites and form propyl radical loosely bond to B-OH. Finally, the formed >B-

O• dangling bond is critical for the subsequent dehydrogenation or activation. The dehydration of B-OH with desorption of water recover the active site and close the catalytic cycle [74]. In summary, It has been frequently reported that the ODHP over hBN is influenced by both heterogeneous (catalyst surface), homogeneous (gas-phase reactions) and co-existence of heterogeneous-homogeneous mechanism (catalytically initiated gas phase reactions via radicals such as C_3H_7• and HOO• desorbing from the hBN surface and reacting in the gas-phase) [48, 52-54, 68].

Based on our observation all of the characterized physicochemical changes during the ODHP reaction over hBN occur without noticeable impact on the catalyst activity, and the stable behavior of hBN was almost preserved in the course of 10 hours under the reaction stream (Figure 28). The catalytic activity of hBN exhibited almost stable behavior in ODHP and showed propane conversion of approximately 25 % with selectivity of ca. 60% toward propene, approximately 17% for both ethene and carbon monoxide, and less than 4 and 2% for methane and carbon dioxide, respectively. Thus, it could be deduced that the boron oxide species that play a key role, are probably formed at the initial states and then the increase in oxygen content is due to formation of other (maybe unimportant) oxygenated boron species or growing the size of boron oxide nanoparticles (or nanoislands on the surface of hBN) that do not interfere in the reaction. However, the experimental evidence of continuously increased boron oxide formation during the ODHP (Figure 21) as well as the enhanced conversion of propane by larger reactors (Figure 26) raised the questions whether the reaction is actually driven by in situ generated boron oxide or the gas-phase chemistry that takes place inside the free space or both. Moreover, whether the free space controls the formation of oxygenated species and subsequently the catalyst activity, or free space and oxygenated species launch as individual phenomena. To answer these questions, two experiments were designed and carried out. The first experiment consisted of three steps: 1: The hBN catalyst was treated in ODHP using a small reactor (9 mm), 2: then the spent catalyst from the small reactor was moved into a larger reactor (15.5 mm), and 3: the spent catalyst from the larger reactor was moved back to the primary small reactor, and in each step the activity of the catalysts was measured in ODHP. As discussed above (Table 4), the fresh catalyst in the small reactor generated a lower oxygen content (3.2 at. %) compared to the larger reactor (15.6 at. %). Therefore, the idea was to see whether the higher content of oxygenated species that was created in the larger reactor results in a higher activity of the catalyst in the smaller reactor or not. The results shown in Figure 29 disclosed that regardless of the amount of oxygen-containing species, the reaction is driven by the empty space because the oxygen content of the spent catalyst in the large reactor which was used for step 3 is five times higher than the oxygen content formed in step 1 using small reactor, but for both steps (1 and 3) the propane conversion is the same (ca. 3%) as the reactor size is identical (9 mm) thus the role of initial oxygenated species is not critical, while the actual driver force is the gas-phase reactions controlled by the free space (**Paper V**).

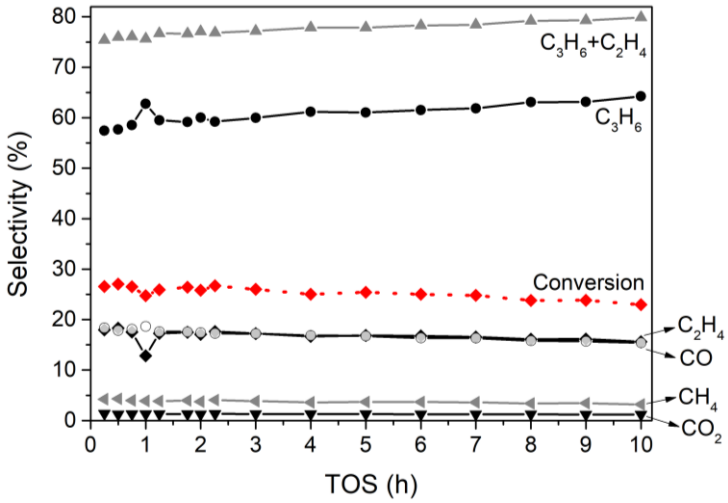

Figure 28. Propane conversion and product selectivity toward products over hBN in ODHP reaction as a function of TOS. Reactor id: 15.5 mm, T: 490 ˚C, mass of catalysts: 100 mg, $He/O_2/C_3H_8$ = 11/3/6 ml min^{-1}

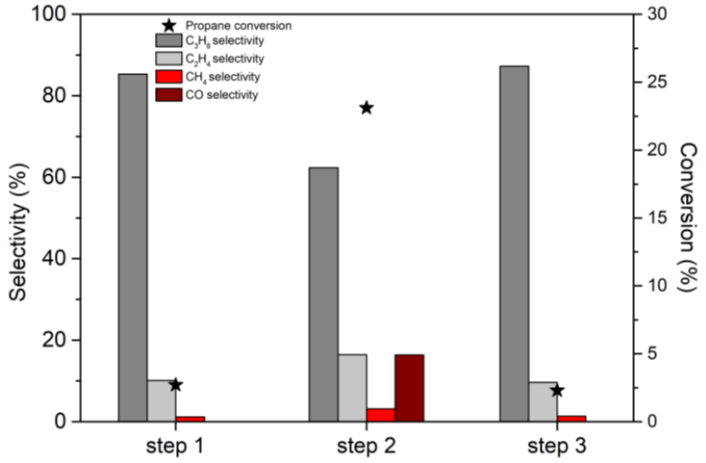

Figure 29. Propane conversion and product selectivity of step 1: fresh hBN in reactor with 9 mm diameter, step 2: the spent hBN from step 1 with O content of 3.2 at. % in reactor with 15.5 mm diameter, step 3: the spent hBN from step 2 with O content of 15.6 at. % in the reactor with 9 mm diameter. The O content after step 3 was measured as 13.7 at. %. T: 490 ˚C, mass of catalysts: 100 mg, TOS: 15 min., $He/O_2/C3H_8$ = 11/3/6 ml min^{-1}

For the second experiment, the catalytic activity of hBN impregnated by boric acid (5 wt.%) was measured in ODHP. Then the catalyst was washed in order to remove the boron oxide and then the catalysts activities were compared (Figure 30). Surprisingly, the impregnated catalyst exhibited 36% less propane conversion compared to fresh hBN, meaning that the pre-formed boron oxide species not only did not improve the activity but also lessened it, probably due to covering the actual active sites or prevention of generating the genuine active sites. After washing the catalyst, the boron oxide was completely removed from the hBN surface and the activity was almost fully recovered. Thus, removing the preformed boron oxide made room for the catalyst to function with the typical access of the gaseous feed to the catalyst surface. The elemental

composition obtained by EDS showed approximately 2 at. % and 12 at. % of oxygen content for the fresh and the impregnated catalyst which decreased to around 2 at. % after washing (Table 5). But interestingly both impregnated and washed catalysts exhibited ca. 12 at. % of oxygen after the reaction, which unveiled that the real active oxygenated species are formed in situ during the reaction and cannot be created by conventional impregnation of boron oxide in advance (**Paper V**). It can be related to the nature of the species or to their sizes. Therefore, these experiments demonstrate that the structure of the active boron oxide is not the same as the preformed added bulk boron oxide. To conclude, the initial amount of boron oxide does not control the reaction pathway but, in fact, the gas-phase reaction is the decisive factor, meaning that the free space, permissible gas-phase reaction chains, and subsequently the interaction of feed with hBN surface for in situ generation of active sites, control the catalytic activity of this system. On the other hand, the activity of the empty reactors without hBN catalyst showed more than 3 % of propane conversion which are only due to formation of radical species in the pure gas-phase reactions. It was also tried to compare the activity of commercial hBN (with 47 m^2/g BET surface area) with a high surface area hBN (with 300 m^2/g BET surface area, and textural properties between microporous-mesoporous isotherms) and the results showed comparable or even a bit lower activity for the high surface area hBN, even though the later one with high BET surface area exhibited ca. 25 at. % oxygen content. Under the same reaction condition, the propane conversion was ca. 18 and 25 % for the high surface area and the commercial hBN, respectively (Figure 31). Likewise, the selectivity toward products were similar. Therefore, these experimental results doubt the previous reports on considering importance of the catalyst surface (in sense how large surface area is) as the initiator of the gas-phase reaction and introduction of the boron oxide species as the main driver (**Paper V**).

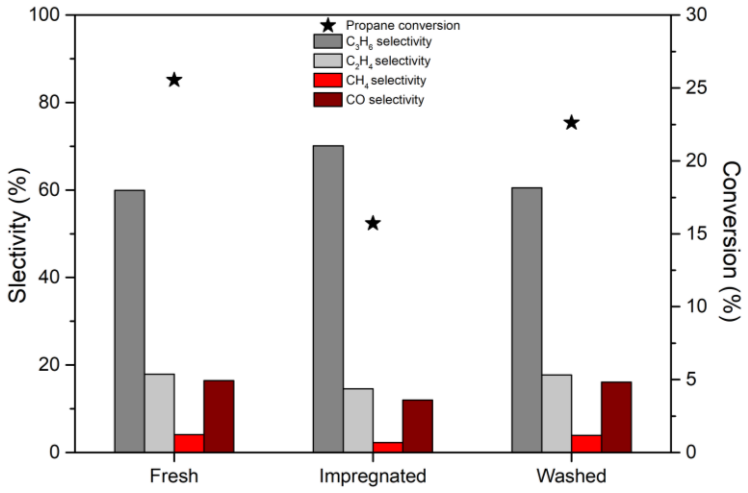

Figure 30. Propane conversion and products selectivity of impregnated BN by boric acid, and after washing, in ODHP, Reactor id: 15.5 mm, T: 490 ˚C, mass of catalysts: 100 mg, TOS: 15 min., $He/O_2/C_3H_8$ = 11/3/6 ml min^{-1}

Table 5. Chemical composition of impregnated and washed hBN before and after the ODHP reaction by EDS.

	Impregnated	washed	Spent impregnated	Spent washed
O at. %	12	2	12	12

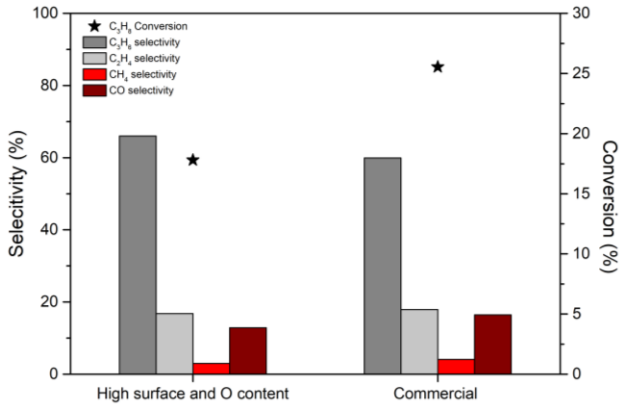

Figure 31. Propane conversion and products selectivity in ODHP over commercial hBN, and the synthesized hBN with higher surface area and oxygen content. T: 490 ˚C, mass of catalysts: 100 mg, TOS: 15 min., $He/O_2/C_3H_8$ = 11/3/6 ml min^{-1}

The effect of dilution was studied in this work and it was observed that the presence of SiC did not improve the activity but in contrary delayed reaching the typical level. This induction period was observed only in the presence of SiC, as the hBN catalyst without dilution exhibited stable activity from the beginning without showing induction time (Figure 32). The total volume of the bed (hBN diluted with SiC) was kept constant while changing the mass of hBN catalyst. Even though the initial activity of different masses of hBN catalyst were not the same, but they all reached similar conversion values after 3h under the stream which is in line with previous data showing that in a constant temperature the free space is the main driving force of the reaction, and as the free space was almost identical, the observed activity was similar. The presence of the induction period could be due to the presence of the diluent, because the radicals and intermediates are quenched on those sites. The slightly higher conversion of the hBN without dilution was probably due to the larger free space. The selectivity towards propene as the main product was a reverse trend of propane conversion and it decreased by time and at the end reached the value of 65 % for all the three diluted hBN catalysts (Figure 33). However, the ethene and CO selectivity increased over time with a similar trend as the propane conversion, and reached ca. 16 % for both after 225 minutes under the stream. The selectivity of the undiluted samples kept the same values due to no change in conversion. The existence of an induction period was reported in another work for ODH of ethane to ethene [75], where the catalyst was also diluted as well, and the selectivity towards ethene decreased gradually by the increase in alkane conversion. In their work, it was claimed that the induction period indicate the B−O site needs to be formed under a certain activation and/or reaction condition, but the effect of the diluent was not considered by them. Because when

we tried the ODH reaction over pure hBN without dilution, our observation did not show any induction period neither for propane nor ethane. Thus, as it was mentioned earlier, the induction can be caused by quenching the generated radicals on the diluent surface and delaying reaching the maximum efficiency. Additionally, an experiment was carried out to demonstrate the activity of hBN in the presence of a fully packed reactor by SiC, to eliminate the entire possible free space of the reactor. The observed conversion was less than 2 % during 3 h of TOS whereas the empty reactor with the same geometry exhibited more than 3 % of propane conversion. Thus, it revealed that the hBN without having available free space is almost inactive in ODHP, and displayed again the critical role of the free space within the reactor for the gas phase reactions as the main driver (**Paper V**). This result contradicts the report by Venegas et al. [54] where addition of SiC improved the propane conversion while the remaining free volume of the reactor was filled by quartz chips. In fact, the presence of a diluent accelerates the radical quenching (based on the type of diluent) which means lowering the extent of reaction, even though the diluents or fillers are chemically inert and will not participate in the reaction. Hence accurate interpretation of the results is always important to not confuse the others working in the same field and we tried to clarify some of those.

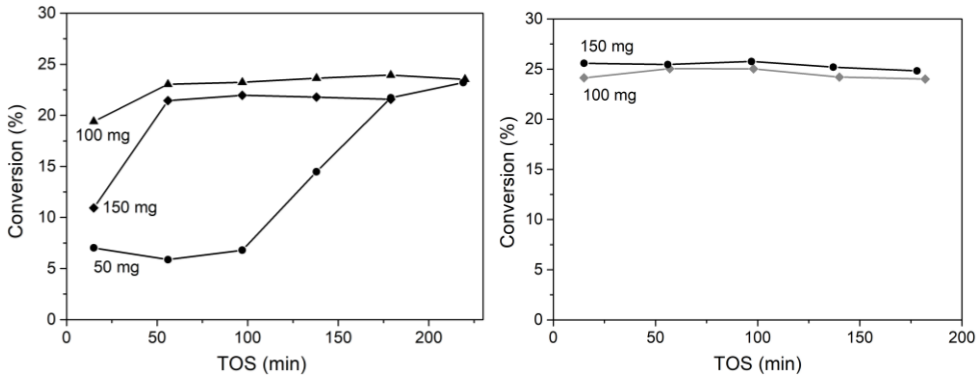

Figure 32. Propane conversion of different hBN masses as a function of time on stream, diluted by SiC (left), undiluted (right). The free volume above the catalyst in reactor with diluted hBN: 5.2 ml, and in reactor without dilution: 5.4 ml for 100 mg and 5.3 ml for 150 mg. Reactor id: 15.5 mm, T: 490 ˚C, $He/O_2/C_3H_8$ = 11/3/6 ml min^{-1}

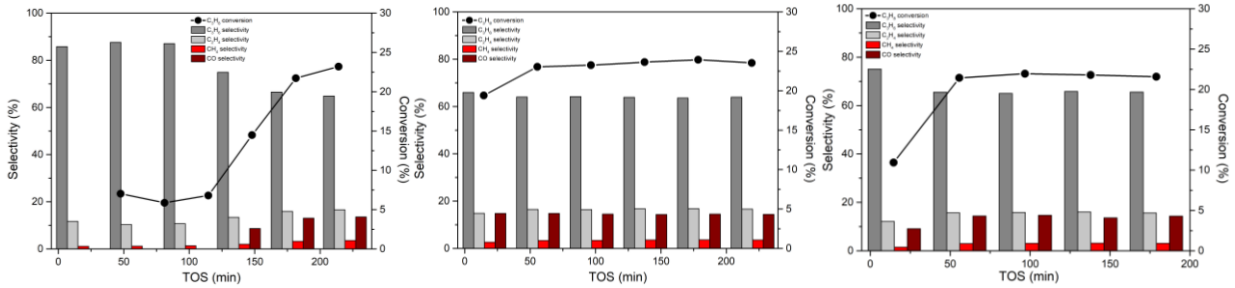

Figure 33. Selectivity towards products for different masses of hBN diluted by SiC, 50 mg (left), 100 mg (middle) and 150 mg (right). The free volume above the catalyst in reactor with diluted hBN: 5.2 ml. Reactor id: 15.5 mm, T: 490 ˚C, $He/O_2/C_3H_8$ = 11/3/6 ml min^{-1}

The pure gas phase reactions which were measured in the reactor with 15.5 mm diameter without the catalyst, exhibited 86 % of propene selectivity and 9 % of ethene selectivity with ca. 3 % propane conversion. The CO, methane and CO_2 selectivity were observed as 0, 3 and 1 % respectively. In comparison with the hBN activity in the reactor of 9 mm diameter with similar propane conversion (ca. 3 %) and under the same reaction condition, it could be seen that the selectivity toward products is just slightly higher and almost comparable. Propene, ethene, CO, methane and CO_2 exhibited selectivity of 85, 11, 2, 0 and 2 % respectively. Therefore, it means in such a situation where there is not enough space for an efficient coupled surface-mediated and gas-phase interaction, the reaction is driven only by the gas phase chemistry. Nevertheless, when hBN activity is measured in the larger reactor (id: 15.5 mm) under the same reaction condition, it is clearly visible that along with the increase in propane conversion to ca. 25 % (and O_2 conversion ca. 80 %), the selectivity to propene decreases to almost 60 % while the cracking products become more selective, such as ethene and CO with 17 % selectivity for both. There is no big change in selectivity toward methane and CO_2 as they stay with 4 and 2 %. However

The effect of catalyst mass on this catalytic system was studied in two different reactors with container diameters of 12.3 mm and 15.5 mm. For both of them, the results showed that the change in catalyst mass did not significantly influence conversion of propane, as shown in Figure 34. Note that changes in the free space were negligible with respect to the different masses of catalyst; therefore, it means the same diameter of catalyst bed provided identical interface between the gas and the solid phase in each reactor, and thus similar free space resulted in a comparable propane conversion (**Paper V**). Even though the experiments involved adjusting the contact time between the gaseous feed and the catalyst surface by varying the mass of hBN, they provided confirmation that the reaction is primarily influenced by the available free space, rather than the quantity of catalyst. The selectivity toward products were similar in the same reactor (Figure 34). In reactor with 12.3 dimeter, for all three masses of hBN, the propene selectivity was kept approximately 74 % ± 2%, and for the ethene and CO ca. 13 ± 1 and 9 ± 1 %. Methane and CO_2 selectivity were less than 2%. In case of the reaction in the reactor with 15.5 mm diameter, both masses of hBN exhibited 61 % ± 2% of propene selectivity, while ethene, CO, and methane selectivity were 17 ± 1, 16 ±1, and 4 ± 0.5 %. CO_2 selectivity was 1%.

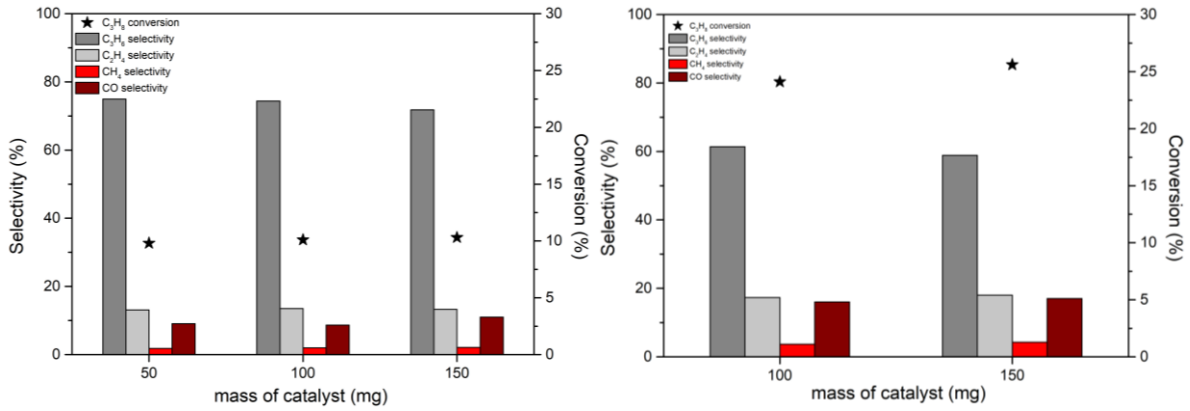

Figure 34. Propane conversion and products selectivity over hBN as a function catalyst mass, reactor diameter: 12.3 mm (left), 15.5 mm (right). The free volume above the catalyst in reactor with 12.3 mm diameter: 50 mg=3.6 ml, 100 mg= 3.4 ml, 150 mg= 3.3 ml, and in reactor with 15.5 mm diameter: 100 mg= 5.4 ml, and 150 mg= 5.3 ml. T: 490 ˚C, $He/O_2/C_3H_8$ = 11/3/6 ml min^{-1}

From the experiments described in the previous paragraphs, the essential role of the free space in the reactor emerges. Therefore, we performed another series of experiments with different values of the total flow rate of the reaction mixture, which affects the contact time with the catalyst as well as the total residence time of the gaseous mixture in the reaction zone of the reactor. It was observed that increasing the total flow rate, which is lowering the contact time and also the residence time of the gas in reactor, resulted in a decrease in the catalyst activity (**Paper V**, and Figure 35). Unlike catalyst mass, that did not play a crucial role in activity (due to not altering the free space), changing total flow within a constant free space, changed the time that the feed molecules (radical species) were able to interact with the hBN surface and/or with each other (residence time), therefore it affected the activity. It could be concluded that both larger free space and lower total flow rate increase the interactions between the gaseous species with each other and also with the catalyst surface and therefore push the ODHP reaction toward higher activity.

In another set of experiments, the propane conversion over the same amount of hBN in the same reactor was measured in the presence of quartz sands (particle size: 0.8-3 mm) as layers occupying one quarter, two quarters, three quarters and four quarters of the free space. The volume of the voids between the particles was calculated based on their porosity. The quartz sand particles occupied 0, 14, 31, 47 and 54 % of the space inside the reactor container. The results showed that by depressing the free space, the conversion rate decreased (Figure 36), which agrees with the observation of the change in the reactor size. Although the free space did not change to zero, because the porosity of the quartz sand layers inside the reactor was quite large, but still when the reactor was filled by the quartz sands, the propane conversion dropped to 2.6 %, because the space between quartz particles as voids were not large enough to let the propagation chain of radicals be formed via gas phase chemistry, and in fact the filler particles turned to a place for termination of the radicals (**Paper V**). As the propane conversion decreases by filling quartz sands, the propene selectivity increases from ca. 61 % for zero filling to 86 % with fully occupied reactor space (Figure 36). In

contrary, the selectivity toward ethene and CO decreases from 17 to 11 and 16 to 0, respectively. Methane selectivity went through a smaller decrease from 4 to 1% while CO_2 selectivity was kept on 1%.

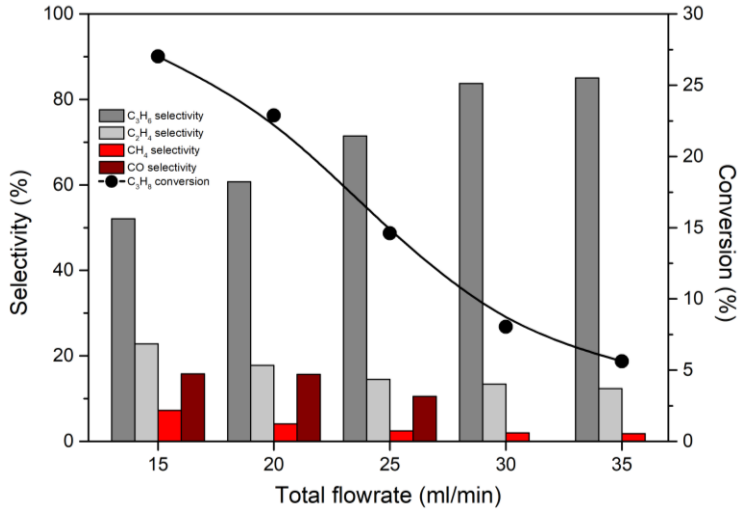

Figure 35. Propane conversion and product selectivity over hBN as a function total flow rate. Reactor id: 15.5 mm, T: 490 ˚C, mass of catalysts: 100 mg, $He/O_2/C_3H_8$ = 55/15/30 %

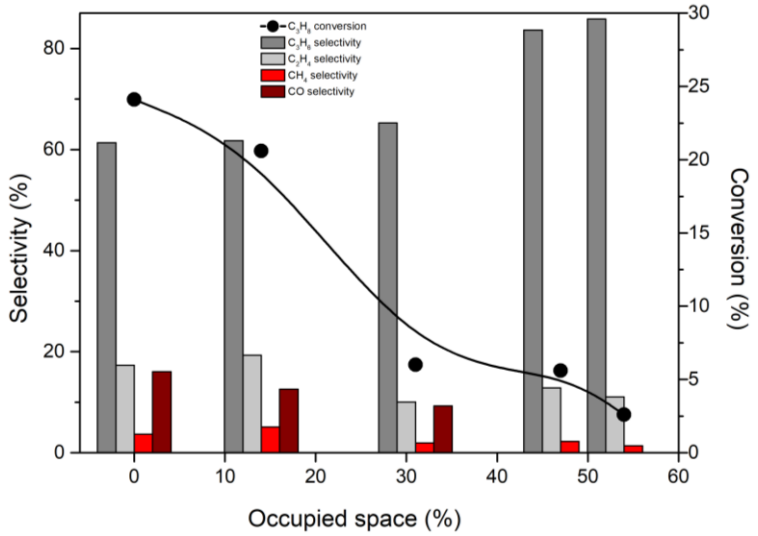

Figure 36. Propane conversion and product selectivity over hBN in ODHP reaction as a function of occupied reactor space by quartz sands. Reactor id: 15.5 mm, T: 490 ˚C, mass of catalysts: 100 mg, $He/O_2/C_3H_8$ = 11/3/6 ml min^{-1}

A combination of results from experiments with changing reactor size, free volume in the reactor by filler and change in flowrate revealed the dependency of reaction rate on residence time shown in Figure 37. It disclosed how propane conversion depends on residence time and supports the hypothesis mentioned above which showed the gas-phase is the main driving force the reaction in this system (**Paper V**).

As the final part of studying hBN behavior, the change in reaction temperature (Figure 38) as well as the changes of products selectivity as a function of conversion were investigated (Figure 39). As it was expected, a higher reaction temperature resulted in higher propane conversion but it also revealed that regardless of how the propane conversion was changed, the selectivity to propene was always a reverse function of the propane conversion, irrespective of whether the size of the reactor was changed, or the temperature, or the amount of catalyst, or the gaseous feed flowrate, etc., the selectivity responded only to the conversion value and possibly took the same pathway. This trend was opposite for the other products which means in the case of ethene, methane and CO, the selectivity increases as the propane conversion was improved.

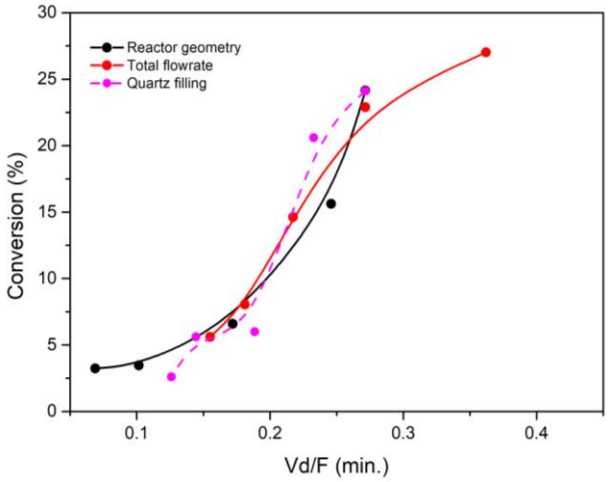

Figure 37. Propane conversion as a function of residence time (free space (or dead volume)/flowrate). Reactor id: 9, 10, 12.3, 14.5 and 15.5 mm, T: 490 ˚C, mass of catalysts: 100 mg, He: O_2: C_3H_8= 55/3/6 %, total flow: 15, 20, 25, 30, 35 ml min^{-1}, quartz filling: 0, 14, 31, 47, 54 %.

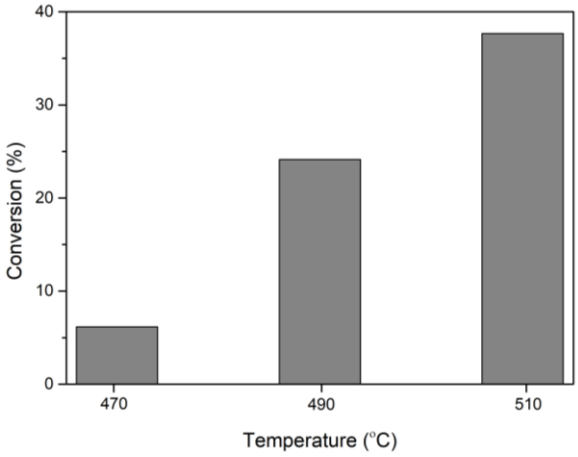

Figure 38. Change of propane conversion in different reaction temperature. Reactor id: 15.5 mm, mass of catalysts: 100 mg, He/O_2/C_3H_8 = 11/3/6 ml min^{-1}

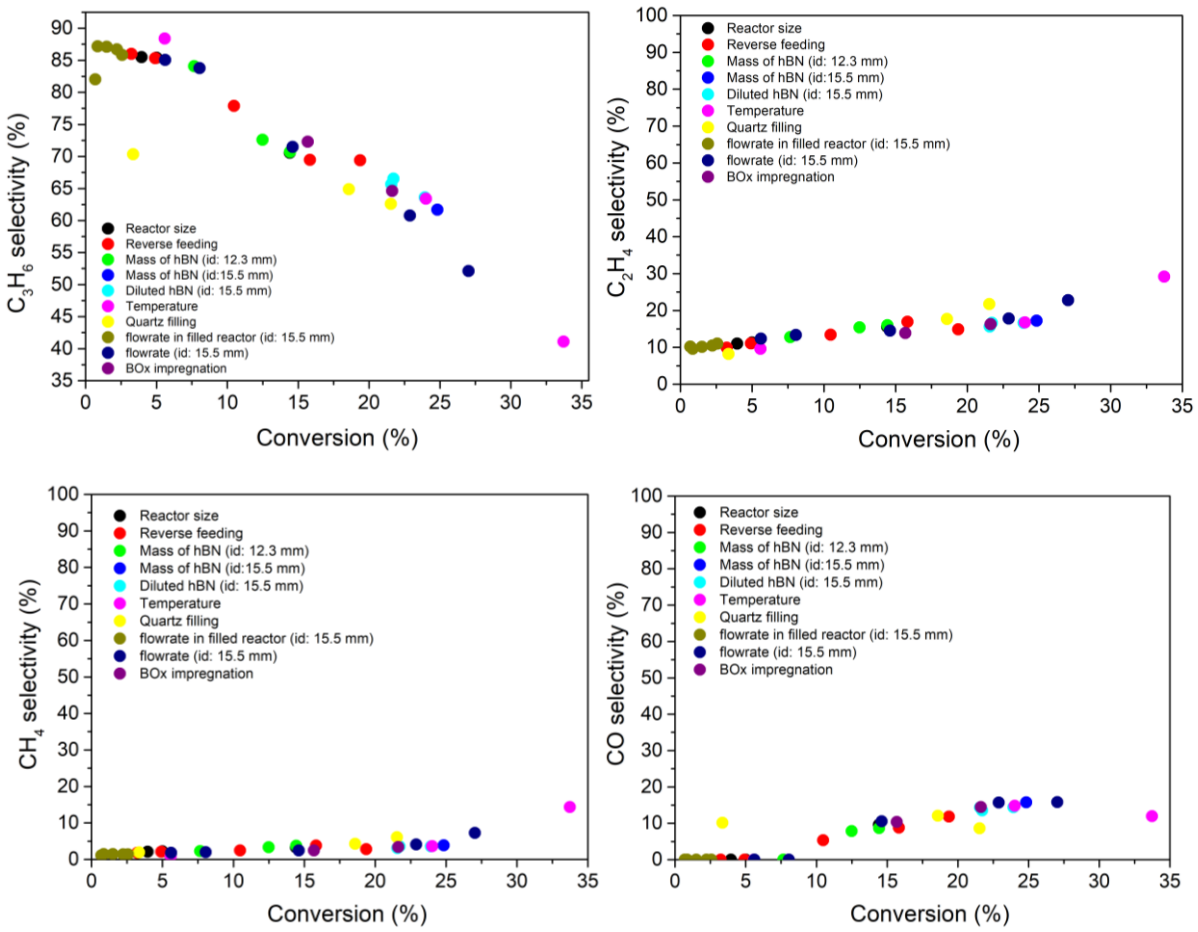

Figure 39. Selectivity towards products as a function of propane conversion.

Herein, the main hypothesis from the literature related to the three topics of reaction initiation, dehydrogenation of propane and selectivity, are discussed and then inspect regarding our observation. In the initiation step, according to the previous studies, the feed molecules are being activated on the surface to form radicals (intermediates), which then continue to propagate in a chain reaction and finally the dehydrogenation of propane takes place [51, 52]. The mixed heterogeneous−homogeneous ODH mechanism has been proposed, which can be described as the boron oxide/hydroxide phase on the surface of the hBN catalyst acting as an initiator to form alkyl radicals, which further react in the gas phase [76]. After oxygen functionalization of boron on the hBN catalyst surface, BO$^{\bullet}$ is formed with the generation of important gas radical HOO$^{\bullet}$ because O_2 could be activated on the catalyst surface and form peroxo-like >BO-OB< species which results in BO$^{\bullet}$ after O-O cleavage. On the other hand, in parallel, the boron surface sites generate B−OH and B−H active species, and then the formed B−H will react with O_2 from HOO$^{\bullet}$, which is the main reactive radical for the gas reaction [53, 76, 77]. Wang et al. [78] proposed different viewpoints, considering the abundant thermodynamically stable B−O−B bridges in tricoordinated B_2O_3

units that could be hydrolyzed to generate more B−OH under ODH conditions. The H abstraction of B−OH occurred in the presence of O_2. The highly reactive species of BO˙ and ˙OOH radicals formed by H abstraction of B−OH by O_2 could invoke the dehydrogenation of propane via the surface channel and gas channel, respectively. The aforementioned reaction processes were reported as the initiation stages during which the radical species are generated.

During the ODHP reaction, the dehydrogenation of propane mainly occurs via the abstraction of hydrogen from propane by the reactive species of BO˙ and ˙OOH radicals [76]. The second hydrogen could be abstracted by the same mean or by O_2. Meanwhile, a part of propene is formed by the direct cleavage of the C−H bond of propyl and isopropyl radicals. As the main byproduct during the ODHP reaction, ethene is mainly derived from C−C bond cleavage and the coupling reaction of C_1 species.

Concerning selectivity, different nature of the propyl radicals was studied to have different effect on selectivity. The n-propyl radicals desorb from the hBN surface favor formation of ethene and CO_x, while iso-propyl radicals are mainly generated during the gas-phase propagation and result in production of propene [56, 57, 68]. By using density functional theory, researchers also suggested that the tricoordinated B−OH could adsorb the oxygenated radicals under ODH conditions, for example, ˙OC_3H_7 and ˙OH, rather than alkyl radicals, for example, ˙C_3H_7, which effectively detained the alkoxy radicals on the surface and freed the alkyl radicals in the gas phase [76-78] and that is the reason for low selectivity to CO_x.

Nevertheless, the experimental results obtained during this study from observation of different characterization of the hBN catalyst under various range of experiments that was discussed during this chapter let us to disagree with some of the previous works and speculate a new pathway. With respect to the reports about how boron sites such as BO, BOH, BH, BOB, etc. are involved in the initiation stage and during the ODHP reaction, then the reaction rate would have to depend also on the amount of the catalyst and/or its specific surface, which is not quite the case as it was shown and discussed earlier. It is clear that the detected oxygenated boron species are not the decisive parameter to form the radicals via boron oxide on the hBN surface (at least for the initiating the reaction), but contrariwise, it seems that the oxygen and propane interaction in the gas-phase form radicals that attack the catalyst surface, and either form the products or generate in-situ boron oxide moieties which could enhance the extent of the reaction. To support this idea, it was shown that the empty reactor without catalyst exhibited some small activity in ODHP reaction. There is a research supporting this hypothesis and results, an old work reporting the reaction of propane and oxygen in the gas-phase taking place at temperature as low as 318 ˚C with product distribution similar to selectivity of the ODH reaction over hBN [79]. Furthermore, our results disclosed that the specific surface area, oxygen content and the amount of hBN catalyst do not play a critical role as far as the available free space is not influenced significantly, because in fact the reaction is driven by the residence time.

Additionally, the hBN catalyst was stable under oxidative atmosphere, therefore the reaction of surface with molecular oxygen is not probable at the reaction temperature. Moreover, it was seen that O_2 molecule was not adsorbed on the surface, monitored by MS, thus oxygen adsorption probably is in dissociative chemisorption pathway. According to this research, the free space role is to provide environment for radical propagation as the main driver of the reaction, and then those radicals could be terminated on the catalyst surface, as products such as propene, water, ethene and methane were desorbed even without presence of oxygen when they were continually detected by MS. Another possible role of hBN might be to terminate radicals on the catalyst surface that results in oxygenated moieties which could enhance the propane conversion.

As this complicated system has attracted increasing attention recently due to its high productivity but meanwhile with complex coupled surface-mediated gas-phase chemistry, there have been numerous controversial works that are confusing for any concrete conclusion. Therefore, this study tried to experimentally clarify the vague points and help to understand the real role of hBN between massive number of proposals, while still more investigations are going on by our group.

CONCLUSION

This thesis focused on a detailed investigation of three catalytic systems that are known to be active for (oxidative) dehydrogenation of light alkanes. Supported alkali chlorides and hBN were studied in the oxidative dehydrogenation of ethane and propane, respectively, while encapsulated Pd NPs within MFI, IPC-2, and IPC-4 zeolites were studied in direct dehydrogenation of propane. The aim was to gain a better understanding of their function, activity, selectivity, stability, physicochemical changes during the reaction, active sites, and involved phenomena. The crucial parameters that define the structural properties of the catalysts as well as the factors that could influence the catalytic behavior or possible deactivation were investigated and discussed in detail on the basis of complex characterization of the fresh and spent catalysts.

It is concluded that although the studied supported alkali chlorides exhibit high selectivity and productivity at relatively low temperature, which was also reported previously, this catalyst suffers from deactivation as a result of chlorine loss. Chlorine is removed from the catalyst in the form of chlorinated hydrocarbons such as chloromethane, ethyl chloride, and chloroethene. Therefore, due to the lack of chlorine, some chlorides convert to oxygenates, which results in the decrease in catalyst activity. The XRD analysis evidenced that $MgCl_2$ is more prone to exchange chlorine for oxygen, thus the activity of the catalyst is tightly connected with the presence of $MgCl_2$. However, it seems that the generation of molten layer salt at the reaction temperature probably provides the conditions for chlorine lability.

Regarding the confinement of Pd NPs within MFI, IPC-2, and IPC-4 zeolites, the results showed that the new approaches used for the encapsulation of metal NPs provided a well distribution of Pd NPs and prevent sintering or leaching of the metal NPs under the reaction condition. Moreover, the encapsulation of metal NPs improved the rate of the desired product formation in all the catalysts compared to that of their impregnated counterparts. Furthermore, the intrinsic activity of Pd NPs with similar size was enhanced by their confinement. Therefore, it is concluded that besides the metal NP size, the activity of Pd NPs is also influence by their interactions with zeolitic support and the structure of pores and channels in the used zeolite. The larger size of metal NPs decrease the metal surface area which has a negative impact on the activity. Nevertheless, the size of zeolite channels, and the structure of the framework play a critical role in mass transfer with diffusion limitations and acceleration of the side reactions such as cracking which should be considered. The Pd NPs encapsulated within IPC-2 and IPC-4 exhibited higher productivity compared to Pd@MFI; nevertheless, it turned out that the ADOR approach, which was used for the encapsulation process of Pd@IPC-2 and Pd@IPC-4, is not a suitable method for zeolites with thin layers such as UTL. The low structural stability of IPC-2 and IPC-4 under the cyclic catalytic test and the tension caused by replacement of Pd NPs resulted in structural collapse.

In the last part, the study of hBN as a promising nonmetallic catalyst in oxidative dehydrogenation of propane revealed that, contrary to the previous reports, the boron oxide species detectable after the reaction do not play the key role. The catalytic activity and selectivity remain almost constant, while the catalyst crystalline phases, textural properties, and chemical composition undergo significant changes mainly due to the presence of oxygenated species within several hours of the reaction. Yet, the results obtained in this investigation revealed that the oxygen content does not control the reaction and in fact the gas-phase chemistry is the main driver in the oxidative dehydrogenation of propane over hBN. Thus, the available free space is a critical parameter because the residence time controls the radical formation/propagation in the gas phase. It could also be stated that the changes in the oxygen content of the catalyst are the result of interaction between activated oxygen in form of radicals and the hBN catalyst. According to our results we can hypothesize that one of the actual roles of hBN catalyst could be to terminate the generated radicals in the gas phase, and form the products. Also, it might result in formation of in situ oxygenated species that ultimately enhance formation of the products. On the other hand, the generated water in the gas phase also can be adsorbed on the hBN surface and produce oxygenated species which might participate in the reaction. Although a final precise mechanism cannot be proposed yet due to the complication of this system, but we have clarified that in contradiction with many reports in the literature, the initiation stage of the reaction in this system is not taking place on the surface of this catalyst, indeed it starts in the gas phase and then the surface contribution comes afterwards.

I believe that these findings helped fill the research gap and that they represent a valuable basis for further investigation of future catalysts as an efficient alternative to traditional catalysts in industrial olefin production as the vital globally required feedstock for chemical industries.

REFERENCES

1. Sattler, J.J.H.B., Ruiz-Martinez, J., Santillan-Jimenez, E., and Weckhuysen, B.M., *Catalytic dehydrogenation of light alkanes on metals and metal oxides.* Chemical Reviews, 2014. 114(20): p. 10613-10653.
2. Sheng, J., Yan, B., Lu, W.-D., Qiu, B., Gao, X.-Q., Wang, D., and Lu, A.-H., *Oxidative dehydrogenation of light alkanes to olefins on metal-free catalysts.* Chemical Society Reviews, 2021. 50: p. 1438-1468.
3. Carter, J.H., Bere, T., Pitchers, J.R., Hewes, D.G., Vandegehuchte, B.D., Kiely, C.J., Taylor, S.H., and Hutchings, G.J., *Direct and oxidative dehydrogenation of propane: from catalyst design to industrial application.* Green Chemistry, 2021. 23(24): p. 9747-9799.
4. Zhang, Y., Yao, W., Fang, H., Hu, A., and Huang, Z., *Catalytic alkane dehydrogenations.* Science Bulletin, 2015. 60(15): p. 1316-1331.
5. Grant, J.T., Venegas, J.M., McDermott, W.P., and Hermans, I., *Aerobic Oxidations of Light Alkanes over Solid Metal Oxide Catalysts.* Chemical Reviews, 2017. 118(5): p. 2769-2815.
6. James, O.O., Mandal, S., Alele, N., Chowdhury, B., and Maity, S., *Lower alkanes dehydrogenation: strategies and reaction routes to corresponding alkenes.* Fuel Processing Technology, 2016. 149: p. 239-255.
7. Liu, J., *Catalysis by supported single metal atoms.* ACS Catalysis, 2017. 7(1): p. 34-59.
8. Zhang, W., Wang, H., Jiang, J., Sui, Z., Zhu, Y., Chen, D., and Zhou, X., *Size dependence of Pt catalysts for propane dehydrogenation: from atomically dispersed to nanoparticles.* ACS Catalysis, 2020. 10(21): p. 12932-12942.
9. Campbell, C.T., *The energetics of supported metal nanoparticles: relationships to sintering rates and catalytic activity.* Accounts of Chemical Research, 2013. 46(8): p. 1712-1719.
10. Campbell, C.T., Parker, S.C., and Starr, D.E., *The effect of size-dependent nanoparticle energetics on catalyst sintering.* Science, 2002. 298(5594): p. 811-814.
11. Farmer, J.A. and Campbell, C.T., *Ceria maintains smaller metal catalyst particles by strong metal-support bonding.* Science, 2010. 329(5994): p. 933-936.
12. Liu, L. and Corma, A., *Metal catalysts for heterogeneous catalysis: from single atoms to nanoclusters and nanoparticles.* Chemical Reviews, 2018. 118(10): p. 4981-5079.
13. Sitja, G., Le Moal, S., Marsault, M., Hamm, G., Leroy, F., and Henry, C.R., *Transition from molecule to solid state: reactivity of supported metal clusters.* Nano letters, 2013. 13(5): p. 1977-1982.
14. Meier, D.C. and Goodman, D.W., *The influence of metal cluster size on adsorption energies: CO adsorbed on Au clusters supported on TiO2.* Journal of the American Chemical Society, 2004. 126(6): p. 1892-1899.
15. Yudanov, I.V., Genest, A., Schauermann, S., Freund, H.-J., and Rösch, N., *Size dependence of the adsorption energy of CO on metal nanoparticles: a DFT search for the minimum value.* Nano letters, 2012. 12(4): p. 2134-2139.
16. Lei, Y., Zhao, H., Rivas, R.D., Lee, S., Liu, B., Lu, J., Stach, E., Winans, R.E., Chapman, K.W., and Greeley, J.P., *Adsorbate-induced structural changes in 1–3 nm platinum nanoparticles.* Journal of the American Chemical Society, 2014. 136(26): p. 9320-9326.
17. Newton, M.A., Belver-Coldeira, C., Martínez-Arias, A., and Fernández-García, M., *Dynamic in situ observation of rapid size and shape change of supported Pd nanoparticles during CO/NO cycling.* Nature materials, 2007. 6(7): p. 528-532.
18. Ou, Z., Li, Y., Wu, W., Bi, Y., Xing, E., Yu, T., and Chen, Q., *Encapsulating subnanometric metal clusters in zeolites for catalysis and their challenges.* Chemical Engineering Journal, 2022. 430: p. 132925.

19. Zhang, Y., Li, A., Sajad, M., Fulajtárová, K., Mazur, M., Kubů, M., Shamzhy, M., Hronec, M., Bulánek, R., and Čejka, J., *Imidazolium-type ionic liquid-assisted formation of the MFI zeolite loaded with metal nanoparticles for hydrogenation reactions.* Chemical Engineering Journal, 2021. 412: p. 128599.
20. Farrusseng, D. and Tuel, A., *Perspectives on zeolite-encapsulated metal nanoparticles and their applications in catalysis.* New Journal of Chemistry, 2016. 40(5): p. 3933-3949.
21. Liu, L., Diaz, U., Arenal, R., Agostini, G., Concepcion, P., and Corma, A., *Generation of subnanometric platinum with high stability during transformation of a 2D zeolite into 3D.* Nature materials, 2017. 16: p. 132-138.
22. Gärtner, C.A., van Veen, A.C., and Lercher, J.A., *Oxidative Dehydrogenation of Ethane: Common Principles and Mechanistic Aspects.* ChemCatChem, 2013. 5(11): p. 3196-3217.
23. Ayari, F., Charrad, R., Asedegbega–Nieto, E., Mhamdi, M., Delahay, G., Farhat, F., and Ghorbel, A., *Ethane Oxidative Dehydrogenation over ternary and binary mixtures of alkaline and alkaline earth chlorides supported on zeolites.* Microporous and Mesoporous Materials, 2017. 250: p. 65-71.
24. Lin, R., Amrute, A.P., and Perez-Ramirez, J., *Halogen-mediated conversion of hydrocarbons to commodities.* Chemical Reviews, 2017. 117(5): p. 4182-4247.
25. Gärtner, C.A., van Veen, A.C., and Lercher, J.A., *Oxidative dehydrogenation of ethane on dynamically rearranging supported chloride catalysts.* Journal of the American Chemical Society, 2014. 136(36): p. 12691-12701.
26. Wang, S.B., Murata, K., Hayakawa, T., Hamakawa, S., and Suzuki, K., *Oxidative dehydrogenation of ethane over alkali metal chloride modified silica catalysts.* Energy & Fuels, 2000. 14(4): p. 899-903.
27. Li, M. and van Veen, A.C., *Selective production of ethylene via continuous oxidative dehydrogenation of ethane in (Dy2O3/MgO)-(Li-K) Cl composite membrane reactor.* Chemical Engineering Journal, 2019. 365: p. 344-350.
28. Zichittella, G., Luthi, J., Paunovic, V., and Perez-Ramirez, J., *Alkane Functionalization via Catalytic Oxychlorination: Performance as a Function of the Carbon Number.* Energy Technology, 2020. 8(8): p. 1900622.
29. Gaab, S., Find, J., Grasselli, R., and Lercher, J., *Oxidative ethane activation over oxide supported molten alkali metal chloride catalysts. Studies in Surface Science and Catalysis*, 2004, Elsevier. p. 673-678.
30. Tope, B., Zhu, Y., and Lercher, J.A., *Oxidative dehydrogenation of ethane over Dy2O3/MgO supported LiCl containing eutectic chloride catalysts.* Catalysis Today, 2007. 123(1-4): p. 113-121.
31. Gärtner, C.A., van Veen, A.C., and Lercher, J.A., *Highly selective supported alkali chloride catalysts for the oxidative dehydrogenation of ethane.* Topics in Catalysis, 2014. 57(14-16): p. 1236-1247.
32. Kristoffersen, H.H. and Metiu, H., *Chemistry of solvated electrons in molten alkali chloride salts.* The Journal of Physical Chemistry C, 2018. 122(34): p. 19603-19612.
33. Zichittella, G., Puértolas, B., Paunović, V., Block, T., Pöttgen, R., and Pérez-Ramírez, J., *Halogen type as a selectivity switch in catalysed alkane oxyhalogenation.* Catalysis Science & Technology, 2018. 8(8): p. 2231-2243.
34. Kristoffersen, H.H. and Metiu, H., *Molten LiCl layer supported on MgO: its possible role in enhancing the oxidative dehydrogenation of ethane.* The Journal of Physical Chemistry C, 2015. 119(16): p. 8681-8691.
35. Kumar, C.P., Gaab, S., Müller, T.E., and Lercher, J.A., *Oxidative dehydrogenation of light alkanes on supported molten alkali metal chloride catalysts.* Topics in Catalysis, 2008. 50(1-4): p. 156-167.
36. Gaab, S., Machli, M., Grasselli, R., and Lercher, J., *Oxidative dehydrogenation of ethane over novel Li/Dy/Mg mixed oxides: structure–activity study.* Topics in Catalysis, 2003. 23(1-4): p. 151-158.
37. Ueda, W., Lin, S.W., and Tohmoto, I., *Highly selective oxidative dehydrogenation of ethane to ethene over layered complex metal chloride oxide catalysts.* Catalysis Letters, 1997. 44(3-4): p. 241-245.

38. Wang, S., Murata, K., Hayakawa, T., Hamakawa, S., and Suzuki, K., *Lithium-chloride-promoted sulfated zirconia catalysts for the oxidative dehydrogenation of ethane.* Catalysis Letters, 1999. 59: p. 173-178.
39. Wang, Z., Chen, L., Zou, G., Luo, X., Gao, R., Chou, L., and Wang, X., *A novel BaCl2–TiO2–SnO2 catalyst for the oxidative dehydrogenation of ethane.* Catalysis Communications, 2012. 25: p. 45-49.
40. Zichittella, G., Aellen, N., Paunović, V., Amrute, A.P., and Pérez-Ramírez, J., *Olefins from natural gas by oxychlorination.* Angewandte Chemie International Edition, 2017. 56(44): p. 13670-13674.
41. Leveles, L., Fuchs, S., Seshan, K., Lercher, J.A., and Lefferts, L., *Oxidative conversion of light alkanes to olefins over alkali promoted oxide catalysts.* Applied Catalysis A: General, 2002. 227(1-2): p. 287-297.
42. Conway, S.J. and Lunsford, J.H., *The oxidative dehydrogenation of ethane over chlorine-promoted lithium-magnesium oxide catalysts.* Journal of Catalysis, 1991. 131(2): p. 513-522.
43. Yu, F., Wu, X., Zhang, Q., and Wang, Y., *Oxidative dehydrogenation of ethane to ethylene in the presence of HCl over CeO2-based catalysts.* Chinese Journal of Catalysis, 2014. 35(8): p. 1260-1266.
44. Weng, Q., Wang, X., Wang, X., Bando, Y., and Golberg, D., *Functionalized hexagonal boron nitride nanomaterials: emerging properties and applications.* Chemical Society Reviews, 2016. 45(14): p. 3989-4012.
45. Grant, J.T., Carrero, C.A., Goeltl, F., Venegas, J., Mueller, P., Burt, S.P., Specht, S.E., McDermott, W.P., Chieregato, A., and Hermans, I., *Selective oxidative dehydrogenation of propane to propene using boron nitride catalysts.* Science, 2016. 354(6319): p. 1570-1573.
46. Shi, L., Wang, D., Song, W., Shao, D., Zhang, W.P., and Lu, A.H., *Edge-hydroxylated Boron Nitride for Oxidative Dehydrogenation of Propane to Propylene.* ChemCatChem, 2017. 9(10): p. 1788-1793.
47. Grant, J.T., McDermott, W.P., Venegas, J.M., Burt, S.P., Micka, J., Phivilay, S.P., Carrero, C.A., and Hermans, I., *Boron and boron-containing catalysts for the oxidative dehydrogenation of propane.* ChemCatChem, 2017. 9(19): p. 3623-3626.
48. Venegas, J.M., McDermott, W.P., and Hermans, I., *Serendipity in catalysis research: Boron-based materials for alkane oxidative dehydrogenation.* Accounts of Chemical Research, 2018. 51(10): p. 2556-2564.
49. Shi, L., Wang, Y., Yan, B., Song, W., Shao, D., and Lu, A.-H., *Progress in selective oxidative dehydrogenation of light alkanes to olefins promoted by boron nitride catalysts.* Chemical communications, 2018. 54(78): p. 10936-10946.
50. Tian, J., Tan, J., Xu, M., Zhang, Z., Wan, S., Wang, S., Lin, J., and Wang, Y., *Propane oxidative dehydrogenation over highly selective hexagonal boron nitride catalysts: The role of oxidative coupling of methyl.* Science Advances, 2019. 5(3): p. eaav8063.
51. Kraus, P. and Lindstedt, R.P., *It'sa gas: Oxidative dehydrogenation of propane over boron nitride catalysts.* The Journal of Physical Chemistry C, 2021. 125(10): p. 5623-5634.
52. Zhang, X., You, R., Wei, Z., Jiang, X., Yang, J., Pan, Y., Wu, P., Jia, Q., Bao, Z., and Bai, L., *Radical Chemistry and Reaction Mechanisms of Propane Oxidative Dehydrogenation over Hexagonal Boron Nitride Catalysts.* Angewandte Chemie International Edition, 2020. 59(21): p. 8042-8046.
53. Venegas, J.M., Zhang, Z., Agbi, T.O., McDermott, W.P., Alexandrova, A., and Hermans, I., *Why Boron Nitride is such a Selective Catalyst for the Oxidative Dehydrogenation of Propane.* Angewandte Chemie International Edition, 2020. 59(38): p. 16527-16535.
54. Venegas, J.M. and Hermans, I., *The influence of reactor parameters on the boron nitride-catalyzed oxidative dehydrogenation of propane.* Organic Process Research & Development, 2018. 22(12): p. 1644-1652.

55. Liu, Y., Liu, Z., Wang, D., and Lu, A.-H., *Suppressing Deep Oxidation by Detached Nano-sized Boron Oxide in Oxidative Dehydrogenation of Propane Revealed by the Density Functional Theory Study.* The Journal of Physical Chemistry C, 2022. 126(50): p. 21263-21271.
56. Liu, Y., Liu, Z., Lu, W.-D., Wang, D., and Lu, A.-H., *In Situ Generated Boron Peroxo as Mild Oxidant in Propane Oxidative Dehydrogenation Revealed by Density Functional Theory Study.* The Journal of Physical Chemistry Letters, 2022. 13: p. 11729-11735.
57. Zhang, Z., Tian, J., Wu, X., Surin, I., Pérez-Ramírez, J., Hemberger, P., and Bodi, A., *Unraveling Radical and Oxygenate Routes in the Oxidative Dehydrogenation of Propane over Boron Nitride.* Journal of the American Chemical Society, 2023. 145(14): p. 7910-7917.
58. Wang, S., Murata, K., Hayakawa, T., and Suzuki, K., *Oxidative Dehydrogenation of Ethane Over Zirconia-Supported Lithium Chloride Catalysts.* Chemical Engineering & Technology: Industrial Chemistry-Plant Equipment-Process Engineering-Biotechnology, 2000. 23(12): p. 1099-1103.
59. Wang, S., Murata, K., Hayakawa, T., Hamakawa, S., and Suzuki, K., *Performance of metal-oxide-promoted LiCl/sulfated-zirconia catalysts in the ethane oxidative dehydrogenation into ethene.* Catalysis Letters, 1999. 62: p. 191-195.
60. *Database of Zeolite Structures: http://www.iza-structure.org/databases/.*
61. Thommes, M., Kaneko, K., Neimark, A.V., Olivier, J.P., Rodriguez-Reinoso, F., Rouquerol, J., and Sing, K.S.W., *Physisorption of gases, with special reference to the evaluation of surface area and pore size distribution (IUPAC Technical Report).* Pure and Applied Chemistry, 2015. 87(9-10): p. 1051-1069.
62. Shi, L., Wang, D., and Lu, A.-H., *A viewpoint on catalytic origin of boron nitride in oxidative dehydrogenation of light alkanes.* Chinese Journal of Catalysis, 2018. 39(5): p. 908-913.
63. Huang, R., Zhang, B., Wang, J., Wu, K.H., Shi, W., Zhang, Y., Liu, Y., Zheng, A., Schlögl, R., and Su, D.S., *Direct insight into ethane oxidative dehydrogenation over boron nitrides.* ChemCatChem, 2017. 9(17): p. 3293-3297.
64. Love, A.M., Thomas, B., Specht, S.E., Hanrahan, M.P., Venegas, J.M., Burt, S.P., Grant, J.T., Cendejas, M.C., McDermott, W.P., and Rossini, A.J., *Probing the transformation of boron nitride catalysts under oxidative dehydrogenation conditions.* Journal of the American Chemical Society, 2018. 141(1): p. 182-190.
65. Huang, M.T. and Ishida, H., *Surface study of hexagonal boron nitride powder by diffuse reflectance Fourier transform infrared spectroscopy.* Surface and Interface Analysis, 2005. 37(7): p. 621-627.
66. Tian, H., Liu, Y., and Xu, B., *Kinetic investigations of oxidative dehydrogenation of propane on boron oxide in confined spaces.* Catalysis Today, 2023. 420: p. 114048.
67. Li, H., Zhang, J., Wu, P., Xun, S., Jiang, W., Zhang, M., Zhu, W., and Li, H., *O2 activation and oxidative dehydrogenation of propane on hexagonal boron nitride: mechanism revisited.* The Journal of Physical Chemistry C, 2019. 123(4): p. 2256-2266.
68. Nadjafi, M., Cui, Y., Bachl, M., Oing, A., Donat, F., Luongo, G., Abdala, P.M., Fedorov, A., and Müller, C.R., *On the Importance of Benchmarking the Gas-Phase Pyrolysis Reaction in the Oxidative Dehydrogenation of Propane.* ChemCatChem, 2023. 15(9): p. e202200694.
69. Altvater, N.R., Dorn, R.W., Cendejas, M.C., McDermott, W.P., Thomas, B., Rossini, A.J., and Hermans, I., *B-MWW Zeolite: The Case Against Single-Site Catalysis.* Angewandte Chemie International Edition, 2020. 132(16): p. 6608-6612.
70. Zhang, Z., Jimenez-Izal, E., Hermans, I., and Alexandrova, A.N., *Dynamic phase diagram of catalytic surface of hexagonal boron nitride under conditions of oxidative dehydrogenation of propane.* The Journal of Physical Chemistry Letters, 2018. 10(1): p. 20-25.
71. Tian, H. and Xu, B., *Oxidative co-dehydrogenation of ethane and propane over h-BN as an effective means for C–H bond activation and mechanistic investigations.* Chinese Journal of Catalysis, 2022. 43(8): p. 2173-2182.

72. Dorn, R.W., Cendejas, M.C., Chen, K., Hung, I., Altvater, N.R., McDermott, W.P., Gan, Z., Hermans, I., and Rossini, A.J., *Structure Determination of Boron-Based Oxidative Dehydrogenation Heterogeneous Catalysts With Ultrahigh Field 35.2 T 11B Solid-State NMR Spectroscopy.* ACS Catalysis, 2020. 10(23): p. 13852-13866.
73. McDermott, W.P., Cendejas, M.C., and Hermans, I., *Recent Advances in the Understanding of Boron-Containing Catalysts for the Selective Oxidation of Alkanes to Olefins.* Topics in Catalysis, 2020. 63: p. 1700-1707.
74. Tian, J., Collinge, G., Yuk, S.F., Lin, J., Glezakou, V.-A., Lee, M.-S., Wang, Y., and Rousseau, R., *Dynamically Formed Active Sites on Liquid Boron Oxide for Selective Oxidative Dehydrogenation of Propane.* ACS Catalysis, 2023. 13(12): p. 8219-8236.
75. Zhou, Y.L., Lin, J., Li, L., Pan, X.L., Sun, X.C., and Wang, X.D., *Enhanced performance of boron nitride catalysts with induction period for the oxidative dehydrogenation of ethane to ethylene.* Journal of Catalysis, 2018. 365: p. 14-23.
76. Gao, X., Liu, M., Huang, Y., Xu, W., Zhou, X., and Yao, S., *Dimensional Understanding of Boron-Based Catalysts for Oxidative Propane Dehydrogenation: Structure and Mechanism.* ACS Catalysis, 2023. 13: p. 9667-9687.
77. Liu, Z., Xu, D., Xia, M., Lu, W.-D., Lu, A.-H., and Wang, D., *Understanding the unique antioxidation property of boron-based catalysts during oxidative dehydrogenation of alkanes.* The Journal of Physical Chemistry Letters, 2021. 12(36): p. 8770-8776.
78. Liu, Z., Lu, W.-D., Wang, D., and Lu, A.-H., *Interplay of on-and off-surface processes in the B2O3-catalyzed oxidative dehydrogenation of propane: a DFT study.* The Journal of Physical Chemistry C, 2021. 125(45): p. 24930-24944.
79. Knox, J.H., *The gaseous products from the oxidation of propane at 318° C.* Transactions of the Faraday Society, 1960. 56: p. 1225-1234.